

# A comparative study of 3D Cumulant and Central Moments lattice Boltzmann schemes with interpolated boundary conditions for the simulation of thermal flows in high Prandtl number regime

G. Gruszczyński<sup>a,b,\*</sup>, Ł. Łaniewski-Wołk<sup>c,a</sup>

<sup>a</sup>*Institute of Aeronautics and Applied Mechanics, Warsaw University of Technology, Warszawa, Poland*

<sup>b</sup>*Interdisciplinary Centre for Mathematical and Computational Modelling, University of Warsaw, Warszawa, Poland*

<sup>c</sup>*School of Mechanical and Mining Engineering, The University of Queensland, St Lucia, Australia*

---

## Abstract

Thermal flows characterized by high Prandtl number are numerically challenging as the transfer of momentum and heat occurs at different time scales. To account for very low thermal conductivity and obey the Courant-Friedrichs-Lewy condition, the numerical diffusion of the scheme has to be reduced. As a consequence, the numerical artefacts are dominated by the dispersion errors commonly known as *wiggles*. In this study, we explore possible remedies for these issues in the framework of lattice Boltzmann method by means of applying novel collision kernels, lattices with large number of discrete velocities, namely D3Q27, and a second-order boundary conditions.

For the first time, the cumulant-based collision operator is utilised to simulate both the hydrodynamic and the thermal field. Alternatively, the advected field is computed using the central moments' collision operator. Different relaxation strategies have been examined to account for additional degrees of freedom introduced by a higher order lattice.

To validate the proposed kernels for a pure advection-diffusion problem, the numerical simulations are compared against analytical solution of a Gaussian hill. The structure of the numerical dispersion is shown by simulating advection and diffusion of a square indicator function. Next, the influence of the interpolated boundary conditions on the quality of the results is measured in the case of the heat conduction between two concentric cylinders. Finally, a study of steady forced heat convection from a confined cylinder is performed and compared against a Finite Element Method solution.

It is known from the literature, that the higher order moments contribute to the solution of the macroscopic advection-diffusion equation. Numerical results confirm that to profit from lattice with a larger number of discrete velocities, like D3Q27, it is not sufficient to relax only the first-order central moments/cumulants of the advected field. In all of the performed benchmarks, the kernel based on the two relaxation time approach has been shown to be superior or at least as good as counter-candidating kernels.

**Keywords:** Heat transfer, Cumulant Lattice Boltzmann Method, Central Moments Lattice Boltzmann Method, interpolated (anti-)bounce-back, high-order moments

---

\*Corresponding author.

Email address: ggruszczyński@gmail.com (G. Gruszczyński)

Preprint submitted to XXX

July 15, 2022

## Nomenclature

| <b>Abbreviations</b>           |   |                    |   |
|--------------------------------|---|--------------------|---|
| <i>ADE</i>                     | advection-diffusion equation              | $\xi$              | continuous particle velocity space  |
| <i>BB</i>                      | bounce-back                               | $\mathbf{e}$       | characteristic lattice velocity   |
| <i>BC</i>                      | boundary condition                        | $\mathbf{u}$       | macroscopic velocity vector   |
| <i>CM</i>                      | central moments                           | $\mathbf{x}$       | position vector   |
| <i>EQ</i>                      | equilibrium scheme                        | $\mathcal{C}$      | forward cumulant transform  |
| <i>FEM</i>                     | finite element method                     | $\mathcal{W}$      | the transformation to <i>moments</i> , <i>central moments</i> or <i>cumulants</i> |
| <i>IABB</i>                    | interpolated-anti-bounce-back             | $\mu$              | dynamic viscosity   |
| <i>IBB</i>                     | interpolated-bounce-back                  | $\nu$              | kinematic viscosity   |
| <i>LB</i>                      | lattice Boltzmann                         | $\Omega$           | collision operator  |
| <i>LBM</i>                     | lattice Boltzmann method                  | $\rho$             | fluid density   |
| <i>MRT</i>                     | multiple relaxation time                  | $\tilde{\Upsilon}$ | central moment of distribution function   |
| <i>NS</i>                      | Navier Stokes                             | $\Upsilon$         | raw moment of distribution function   |
| <i>SRT</i>                     | single relaxation time                    | $c$                | cumulant of distribution function   |
| <i>TRT</i>                     | two relaxation time                       | $c_s$              | lattice speed of sound  |
| <b>Dimensionless Variables</b> |   | $D$                | diameter  |
| <i>Nu</i>                      | Nusselt number                            | $f_i$              | i-th distribution function for velocity field                                     |
| <i>Pr</i>                      | Prandtl number                            | $g$                | distribution function of interest   |
| <i>Re</i>                      | Reynolds number                           | $H$                | internal energy   |
| <b>Superscripts</b>            |   | $h_i$              | i-th distribution function for internal energy field                              |
| $\sim$                         | quantity in central moment space          | $k$                | thermal conductivity  |
| $\star$                        | post collision quantity                   | $L$                | length of the domain  |
| <i>eq</i>                      | equilibrium                               | $lu$               | lattice unit  |
| $H$                            | quantity related to internal energy field | $N$                | number of spatial dimensions  |
| <b>Symbols</b>                 |   | $q$                | number of discrete velocities   |
| $\mathbb{M}$                   | transformation matrix                     | $s_i$              | i-th relaxation frequency   |
| $\mathbb{N}$                   | shift matrix                              |                    |   |
| $\mathbb{S}$                   | relaxation matrix                         |                    |   |

## 1. Introduction

The advection-diffusion equation (ADE) may be viewed as a key building block in CFD modelling. In its simplest form, it describes the transport of scalar fields such as temperature,

or concentrations of different chemical components across the spatial domain. The equation can be extended by addition of a source terms to account for chemical reactions, or heat generation. Once the density of a medium is introduced, the energy transfer can be properly modelled. Finally, a much more complex, nonlinear Navier Stokes (NS) equation describe the motion of a fluid.

Several numerical methods are currently used across both academia and industry for solving both the Navier Stokes and advection-diffusion equations. These include, but are not confined to, finite difference, finite volume [1], and finite element method (FEM) [2], which all discretise the macroscopic equations directly. Alternatively to solving discretised macroscopic equations, the lattice Boltzmann method (LBM) focuses on the evolution of a distribution function. The distribution function define the density of some macroscopic physical quantity (such as mass or chemical concentration) across space. From the microscopic perspective, it can be viewed as the probability of finding a quantity-carrying particle with a given velocity and coordinates at a given time. In the discretised form, the set of velocities is finite. In each iteration, the discretised distributions are passed to neighbouring nodes along these velocities, in a step called streaming. This requires exchange of information with neighbouring nodes. Next, a local collision step is performed in each node, which relaxes the distribution function toward some form of an equilibrium.

During the last decades, a variety of collision operators have been proposed. For the detailed discussion of this subject, the reader is referred to the comparative works [3–5] and established textbooks [6, 7]. In the recent years, a substantial effort was made to use the mutual independence of the observable quantities (such as density, momentum, stress tensor components, etc.) to separate their relaxation frequencies and improve stability. In the simplest form of the collision operator, a single relaxation time (SRT) is assigned to all distribution functions. The next concept follows from the fact that the observable quantities can be found as moments of the distribution function [6, 8]. As different relaxation rates can be assigned to each moment, the multiple relaxation time (MRT) name has been coined [8]. The moments can be calculated in stationary or moving reference frame and are refereed as raw or central moments (CM) respectively [9]. A method, in which the relaxation rates of odd and even raw moments are separated has been originally proposed by Ginzburg [10], and is known as two relaxation time (TRT).

The proper choice of the combination of moments used during the collision step plays important role for the stability of the scheme. Dubois et al. [11] have benchmarked two frequently used sets in the contexts of NS equations. Some researchers argue that the orthogonalisation of the transformation from distribution function to the moments' space shall limit the *cross-talk* between the moments [12]. On the other hand Geier et al. [13, Appendix I] stated that the orthogonalisation process can be the source of spurious couplings. The article proposed that a more complex, non-linear, statistically independent quantities known as cumulants can be calculated from the distribution function. Their use in the LBM framework resulted in the formulation of the Cumulant Lattice Boltzmann Method, which exhibited very promising numerical properties [13, 14].

The Prandtl number ( $Pr$ ) defines the ratio of kinematic viscosity to thermal diffusivity. Modelling high  $Pr$  flows rises numerical difficulties due to different time scales of the physical phenomena occurring in the hydrodynamic and thermal field. Briefly, three distinct approaches to model thermal flows within the LBM framework can be distinguished in the literature [15].

In a *fully coupled double distribution function* approach, a second distribution function evolving between the same lattice nodes, at the same timesteps as the hydrodynamic one, is introduced to simulate the evolution of the energy field [16]. Due to tight coupling, many benchmarks pub-

lished for this type of LBM models are restricted to  $Pr \leq 100$  [17–19] or  $Pr \approx 1$  [16, 20–34]. Limits of this way of modelling, are explored in the current paper.

Another approach, called multispeed LBM uses single distribution function, but utilises a lattices with a large velocity set [35]. The expanded velocity set allows to eliminate the aliasing of the higher order moments of the distribution. As a result, the internal energy can be incorporated as a quantity solved by LBM. This is not possible for standard lattices, as the limited number of independent moments results in a fixed relation between the internal energy and the pressure, which is referred as *isothermal LBM*. The use of the multispeed method with the SRT collision operator would lead to the  $Pr$  being a constant of the model, as the relaxation rate corresponding to the thermal conductivity could not be set independently of from the kinematic viscosity [36, 37]. Successful decoupling has been achieved by Chen et al. [38] followed by Shan [39]. A collision operator with multiple relaxation frequencies in a moving reference frame has been proposed and validated for  $Pr \in \{0.5, 1, 2\}$ .

In the hybrid approach, two distinct numerical methods are used to solve the hydrodynamics and the advected field. Examples of this approach include studies, where LBM solver was used for the NS equations and a finite difference [40, 41] or finite volume [31] method for the thermal field.

Finally, some researches attempt to take advantage of high  $Pr$  regime to decouple NS and ADE solvers. In this method, both fields can be computed using LBM solver, but on separated lattices [42, 43]. Parmigiani et al. [42] notes that either the timestep or grid spacing of the second distribution can be decoupled. Although the spatial decoupling demands interpolations between lattices, the overall computational cost is reduced. The group managed to simulate flow with  $Pr$  up to 1000. However, when the heat transport becomes velocity controlled, the advantages of decoupling deteriorate [42].

Discretisation of the velocity space in the Lattice Boltzmann Method corresponds to the number of links between each of the neighbouring nodes in the lattice. In general, the choice of the discrete velocity set is dictated by the target macroscopic equation. On the one hand, large velocity sets are expected to provide more accurate [21] and stable solutions [44]. On the other hand, they contribute to increased memory consumption, computational and communication cost, as well as complexity of boundary conditions. The velocity sets are commonly described using  $DdQq$  notation, where  $d$  corresponds to the number of spatial dimensions and  $q$  accounts for the number of discrete velocities. The  $Q_F$  and  $Q_H$  subscripts will be used in the present work to distinguish the lattices used for hydrodynamic and thermal distribution functions, hence defining the lattice as  $DdQ_F \times Q_H$ .

To solve the advection-diffusion equations, a lower order lattices like  $D2Q_H5$  [25–27, 29] and  $D3Q_H7$  [32, 34, 45–50] are frequently used. However, to properly recover complex thermal flows (e.g. measure the critical Rayleigh number), a higher-order lattice is required [21]. According to Huang et al. [51], the accuracy of  $D2Q_H4$ ,  $D2Q_H5$  and  $D2Q_H9$  lattices can be comparable, but the effects of low diffusivity were not considered in their study. Additionally, lattices such as  $D3Q15$  shall be avoided, as it is not feasible to derive the shift matrix from the raw moment space (discussed in next section) following the procedure presented by Asinari [52]. Apart from increasing the number of discrete velocities, it is possible to take advantage of a specific geometry of the problem by either scaling a lattice into cuboidal one [53] or by adding a correction terms to account for axisymmetric flows [54]. Interestingly, when the relaxation frequency is exactly equal to one, a memory efficient LBM scheme can be implemented, by eliminating the storage of the distribution function. From the theoretical perspective, a memory savings of up to  $\sim 86\%$  can be achieved for the  $D3Q27$  lattice [55].

In the current study, a linear interpolation scheme [56] is implemented to represent a boundary located between lattice nodes and improve the representation of the geometry. Readers interested in a more detailed studies on the application of an interpolated-anti-bounce-back boundary condition are referred to [57–60].

Application of standard lattices, such as  $D2Q_H9$  [61] and  $D3Q_H15$  [62], -19 or -27, raises the question of the appropriate relaxation of higher-order moments. Due to its simplicity, the SRT collision operator is frequently applied [17, 18, 20–22, 48, 49, 63–68]. When it comes to use a more advanced MRT [22, 23, 32, 34, 45, 47, 69–71] or CM [25–27, 54, 61, 62, 72] collision operator, various relaxation strategies can be identified. Some authors [23, 34, 45, 47, 61, 62, 70] relax first-order moments only, setting the rest of moments to their corresponding equilibrium values. The TRT approach was adopted to moment space [22, 32, 69] and central moment space in [26, 27, 72], however in [61, 62, 72] the relaxation of higher-order moments is said to be tunable.

It has been shown by different authors [35, 72–75], that truncation of the equilibrium distribution function deteriorates Galilean invariance of the flow model. Chopard et al. [76] have discussed the role of the second-order velocity terms in the equilibrium distribution function on the error of the recovered macroscopic equation and proposed a correction term. Nie et al. [35] noticed that the error appears as spurious dependence of the macroscopic diffusion coefficient (i.e. viscosity or thermal conductivity) on velocity. A similar effect has been observed by Fei et al. [72] who used a cascaded collision operator with full order equilibrium to show that thermal diffusivity is independent of Mach number as opposed to works where MRT with truncated equilibrium [71, 77] were used. To avoid the above-mentioned issues, a full order equilibrium distribution function is used in the present work.

The Table 1 presents a concise summary of the models present in the literature, to put the collision operators chosen in this work in a context. Features such as the type of collision kernel, order of equilibrium, utilized lattice and the range of reported Prandtl numbers has been extracted. The publications were usually focused only on selected properties from the aforementioned set. Usage of SRT collision and truncated equilibrium distribution is prevalent, as is the relaxation of only first raw, or central moments. It is expected that to some extend, the models listed in Table 1 would work for Prandtl numbers other than reported.

In this contribution, the role of different relaxation approaches for the advection-diffusion problems is investigated. To the best of the authors' knowledge a cumulant collision kernel is applied to simulate the advection-diffusion equation for the first time. A set of benchmarks with different complexity has been conducted, to isolate the factors which can affect the numerical simulations. For the set of numerically investigated cases, specified for a range of non-dimensional numbers, the relaxation of higher-order moments has to be adjusted to achieve the benefits of lattice with a large stencil. Concluding, current work is focused on the numerical limits of the central moment and cumulant collision operators applied to the variant of advection-diffusion equation, namely transport of internal energy in a homogeneous, isotropic medium with first and second-order boundary conditions using a fully coupled double distribution function approach on a  $D3Q_F27Q_H27$  lattice.

This paper is organised as follows. In the Section 2, the LBM routine and the investigated collision kernels are described. In Section 3, the interpolated boundary conditions, which allow to better represent walls location, are presented. The validation and tests of the model is discussed in Section 4. The future outlook is given in Section 5. Finally, the summary and conclusions are formulated in Section 6. For clarity of the manuscript, some of the derivations regarding discretisation of the distribution function, two relaxation time approach, the transformation ma-

| Year | Reference                      | Notes | Collision           | $h^{eq}$ ord.   | Lattice     | $Pr$      |
|------|--------------------------------|-------|---------------------|-----------------|-------------|-----------|
| 1998 | He et al. [16]                 |       | SRT                 | 2 <sup>nd</sup> | D2Q9        | 0.25÷0.71 |
| 2007 | Guo et al. [20]                |       | SRT                 | 2 <sup>nd</sup> | D2Q9        | 0.71÷1    |
| 2009 | Parmigiani et al. [42]         | (a)   | SRT                 | 1 <sup>st</sup> | D2Q5        | 10÷1000   |
| 2010 | Yoshida and Nagaoka [45]       |       | MRT-1 <sup>st</sup> | 1 <sup>st</sup> | D3Q7        | —         |
| 2013 | Huang et al. [64]              |       | SRT                 | 2 <sup>nd</sup> | D2Q9        | 0.02      |
| 2013 | Karlin et al. [78]             |       | Entropic            | 2 <sup>nd</sup> | DdQq        | 1         |
| 2013 | Wang et al. [69]               |       | MRT-TRT             | 1 <sup>st</sup> | D2Q5        | 0.71÷7    |
| 2014 | Chen et al. [38]               | (b)   | CM-TRT              | 4 <sup>th</sup> | D2Q27       | 0.5÷2     |
| 2014 | Yoshida et al. [47]            |       | MRT-1 <sup>st</sup> | 1 <sup>st</sup> | D3Q7        | —         |
| 2015 | Huang and Wu [22]              |       | MRT-TRT             | 2 <sup>nd</sup> | D2Q9        | 0.2       |
| 2015 | Feng et al. [21]               |       | SRT                 | 2 <sup>nd</sup> | D3Q15/19/27 | 0.71      |
| 2016 | Li et al. [23]                 | (c)   | MRT-1 <sup>st</sup> | 1 <sup>st</sup> | D3Q7        | 0.71      |
| 2017 | Sharma et al. [25]             |       | CM-TRT              | ∞               | D2Q5        | 0.71      |
| 2017 | Xu et al. [79]                 | (e)   | MRT-TRT             | 1 <sup>st</sup> | D2Q5        | 0.71      |
| 2017 | Lu et al. [67]                 |       | SRT                 | 2 <sup>nd</sup> | D2Q9        | 1         |
| 2018 | Sharma et al. [26]             |       | CM-TRT              | ∞               | D2Q5        | 0.71      |
| 2018 | Fei and Luo [28]               |       | SRT                 | 2 <sup>nd</sup> | D2Q9        | 0.71      |
| 2018 | Feng et al. [31]               |       | SRT                 | 2 <sup>nd</sup> | D2Q9        | 0.71      |
| 2018 | Hajabdollahi and Premnath [62] |       | CM-1 <sup>st</sup>  | ∞               | D3Q15       | 0.71      |
| 2018 | Elseid et al. [61]             |       | CM-1 <sup>st</sup>  | ∞               | D2Q9        | 0.71÷1    |
| 2018 | Fei and Luo [27]               | (d)   | CM-TRT              | ∞               | D2Q5        | 0.71      |
| 2018 | Lu et al. [29]                 |       | MRT-TRT             | 2 <sup>nd</sup> | D2Q9        | 0.7÷1     |
| 2019 | Hosseini and Thevenin [30]     |       | SRT                 | 1 <sup>st</sup> | D2Q9        | 0.7÷1     |
| 2019 | Shan [39]                      | (b)   | CM-TRT              | 9 <sup>th</sup> | D2Q37       | 0.5       |
| 2019 | Xu et al. [32]                 |       | MRT-TRT             | 1 <sup>st</sup> | D3Q7        | 0.7÷7     |
| 2019 | Sajjadi et al. [34]            | (c)   | MRT-1 <sup>st</sup> | 1 <sup>st</sup> | D3Q7        | 0.73      |
| 2019 | Lu et al. [80]                 |       | MRT-TRT             | 2 <sup>nd</sup> | D2Q9/D3Q7   | 0.02      |
| 2019 | Yip et al. [33]                |       | SRT                 | 1 <sup>st</sup> | D2Q5        | 0.2       |
| 2020 | Mabrouk et al. [17]            |       | SRT                 | 1 <sup>st</sup> | D2Q9        | 50        |
| 2021 | Du et al. [18]                 |       | SRT                 | 2 <sup>nd</sup> | D2Q9        | 50        |
| 2021 | Chen et al. [19]               |       | SRT                 | 1 <sup>st</sup> | D3Q7        | 100       |
| 2021 | Nabavizadeh et al. [43]        | (a)   | SRT                 | 1 <sup>st</sup> | D2Q9        | 0.01÷100  |
| 2022 | current model                  |       | CM-TRT              | ∞               | D3Q27       | 10÷1000   |

Table 1: The summary of models present in the literature.  $h^{eq}$  ord. - Order of equilibrium distribution function used for the advection-diffusion equation (value  $\infty$  means that equilibrium is not truncated, **Pr** - Prandtl number. Notes: a - NS and ADE were computed on decoupled lattices, b - multispeed model, c - collision based on [45], d - collision based on [71], e - collision based on [69]. The  $\div$  sign is used to indicate the range of  $Pr$  for which the model has been benchmarked. The — sign means that the definition of  $Pr$  does not apply, i.e. the model was presented for advected field only.

trices and the source treatment have been listed in [Appendix A](#), [Appendix B](#), [Appendix C](#) and [Appendix D](#) respectively.

## 2. Model description

In the present study, the flow of fluid and internal energy balance is modelled by the Navier-Stokes and advection-diffusion equation respectively. Only one-way coupling between these equations will be considered. The hydrodynamics is described by the continuity and momentum equations,

$$\frac{\partial \rho}{\partial t} + \nabla \cdot \rho \mathbf{u} = 0, \quad (1)$$

$$\rho \left( \frac{\partial \mathbf{u}}{\partial t} + (\mathbf{u} \cdot \nabla) \mathbf{u} \right) = -\nabla p + \nabla \cdot (\mu [\nabla \mathbf{u} + (\nabla \mathbf{u})^T]), \quad (2)$$

where  $\mathbf{u}$  is the fluid velocity,  $\rho$  is the density,  $p$  is pressure, and  $\mu$  is the viscosity coefficient. Although the LBM is a weakly compressible method, it is used in this study in the incompressible regime ( $\rho \simeq \text{const}$ ).

The heat transfer is described using an internal energy field expressed as  $H = \rho c_v T$ , where  $c_v$  is a specific heat capacity at constant volume and  $T$  is the temperature. Omitting viscous heat production and assuming that the flow is incompressible, the conservation of internal energy can be written as [15, 81, 82],

$$\frac{\partial}{\partial t} (\rho c_v T) + \nabla \cdot (\mathbf{u} \rho c_v T) = \nabla \cdot (k \nabla T), \quad (3)$$

with thermal conductivity of the fluid being denoted by  $k$ . As the conjugate heat transfer in the surrounding medium is not considered in this study, the  $c_v$  is set to 1. Having calculated the velocity field from Eqs. (1) and (2), the advection-diffusion of  $H$  can be solved independently. Readers interested in the Chapman-Enskog procedure for the advected field are referred to the work of Shi et al. [81].

### 2.1. Lattice Boltzmann Method

The basic principles of the LBM can be found in a book by Krüger et al. [6] or Succi [7]. This section will present the relevant details of the procedure, needed to understand the differences between different collision operators used.

The fluid flow and temperature field in the present LBM framework is described with two distributions functions,  $f_\alpha$  and  $h_\alpha$ , with the corresponding set of velocity vectors  $\mathbf{e}_\alpha$ . The connection between  $\mathbf{f}$  and  $\mathbf{h}$ , and macroscopic flow fields is described by,

$$\rho = \sum_{\alpha} f_{\alpha}, \quad (4)$$

$$\rho \mathbf{u} = \sum_{\alpha} \mathbf{e}_{\alpha} f_{\alpha}, \quad (5)$$

$$\rho c_v T = \sum_{\alpha} h_{\alpha}. \quad (6)$$

The general evolution equation of these distributions can be decomposed into two steps: collision and streaming. The collision is a nonlinear operator  $\Omega$  acting on the distribution function at a specific time and location, while the streaming spreads this distribution function along the velocity vectors  $\mathbf{e}_\alpha$ . This is expressed as,

$$f_\alpha(\mathbf{x} + \mathbf{e}_\alpha \delta t, t + \delta t) = \Omega_{F,\alpha}(\mathbf{f}(\mathbf{x}, t)), \quad (7)$$

$$h_\alpha(\mathbf{x} + \mathbf{e}_\alpha \delta t, t + \delta t) = \Omega_{H,\alpha}(\mathbf{h}(\mathbf{x}, t)). \quad (8)$$

The formulations of the LBM are presented for the D3Q27 lattice, as restrictions to smaller lattice or to two dimensions can be easily derived using the presented formulas. Using the Euclidean basis, the discrete velocities for a D3Q27 lattice read,

$$\mathbf{e} = [\mathbf{e}_x, \mathbf{e}_y, \mathbf{e}_z], \quad (9)$$

$$\mathbf{e}_x = [0, 1, 0, 0, 1, 1, 0, -1, 0, 0, 1, 1, -1, -1, 0, 0, 1, -1, -1, 0, -1, 1, 1, 1, -1, -1, -1]^\top, \quad (10)$$

$$\mathbf{e}_y = [0, 0, 1, 0, 1, 0, 1, 0, -1, 0, -1, 0, 1, 0, 1, -1, 1, -1, 0, -1, 1, -1, 1, -1, 1, -1, -1]^\top, \quad (11)$$

$$\mathbf{e}_z = [0, 0, 0, 1, 0, 1, 0, 1, 1, 0, 0, -1, 0, -1, 0, 1, -1, 1, 1, 0, -1, -1, 1, 1, -1, -1, -1, -1]^\top. \quad (12)$$

In general, a different set of velocity vectors  $\mathbf{e}$  can be chosen for the evolution of  $\mathbf{f}$  and  $\mathbf{h}$ .

As many equations are formulated analogously for both  $\mathbf{f}$  and  $\mathbf{h}$ , the letter  $\mathbf{g}$  will be used as placeholder for both of these distribution functions. In this study, the collision operator  $\Omega$  is considered to consist of three steps: some transformation  $\mathcal{W}$ , relaxation to equilibrium, and inverse of the transformation,

$$\Omega_G(\mathbf{g}) = \mathcal{W}^{-1}(\mathcal{W}(\mathbf{g}) + \mathbb{S}(\mathcal{W}(\mathbf{g}^{\text{eq}}) - \mathcal{W}(\mathbf{g}))), \quad (13)$$

where  $\mathbb{S}$  is the relaxation matrix. The operator  $\mathcal{W}$  can be the transformation to the space of *moments*, *central moments* or *cumulants*.

The moments of distribution function can be calculated in a stationary or a moving reference frame [9]. The so-called *cascaded* or central moments are moments calculated in a reference frame, moving with the local macroscopic velocity,  $\mathbf{u}$ . The discrete, raw and central moments are defined as,

$$\Upsilon_{mno}^G = \sum_\alpha (e_{\alpha x})^m (e_{\alpha y})^n (e_{\alpha z})^o g_\alpha, \quad (14)$$

$$\tilde{\Upsilon}_{mno}^G = \sum_\alpha (e_{\alpha x} - u_x)^m (e_{\alpha y} - u_y)^n (e_{\alpha z} - u_z)^o g_\alpha, \quad (15)$$

where  $mno$  is a three-index, spanning triplets of positive numbers. Notice, that for a fixed set of three-indexes  $mno$ , the Eqs. (14) and (15) forming the raw,  $\mathcal{M}$ , and central moment,  $\tilde{\mathcal{M}}$ , transforms can be expressed as matrix multiplication [52, 83, 84],

$$\Upsilon^G = \mathcal{M}(\mathbf{g}) = \mathbb{M}\mathbf{g}, \quad (16)$$

$$\tilde{\Upsilon}^G = \tilde{\mathcal{M}}(\mathbf{g}) = \mathbb{N}\Upsilon^G, \quad (17)$$

where  $\Upsilon$  and  $\tilde{\Upsilon}$  denote the vector containing raw and central moments, respectively. Here, we select all indexes  $mno$  for which  $m$ ,  $n$  and  $o$  are less than 3, in the following order: [000, 100, 010, 001, 110, 101, 011, 200, 020, 002, 120, 102, 210, 201, 012, 021, 111, 220, 202, 022, 211, 121, 112, 122, 212, 221,



222 ]. This choice of 27 moments results in non-singular square matrices  $\mathbb{M}$  and  $\mathbb{N}$ , making the  $\mathcal{M}$  and  $\tilde{\mathcal{M}}$  operators reversible. Remarks regarding assembling of the matrices can be found in [Appendix C](#).

The density and internal energy correspond to the zeroth order moments of hydrodynamic and energy distribution functions respectively. The momentum  $\rho\mathbf{u}$  corresponds to the first moment of  $\mathbf{f}$ . According to the probabilistic definition, the cumulants or central moments of some quantity  $\mathbf{g}$  shall be calculated basing on  $\mathbf{g}$  itself. Observe, that the *cascaded* or central moments, defined here, would correspond to the probabilistic definition of central moments in case hydrodynamics distributions,  $\mathbf{f}$ , but do not for the advected ones,  $\mathbf{h}$ . Strictly speaking, the macroscopic velocity,  $\mathbf{u}$ , being used to compute the shift matrix,  $\mathbb{N} = \mathbb{N}(\mathbf{u})$ , is related to the first order moment of  $\mathbf{f}$  not  $\mathbf{h}$ .

A detail presentation of the cumulant transformation,  $\mathcal{C}$ , and the use of cumulants in LBM, can be found in the works of Geier [13, 14] and Coreixas [4, 5]. In this work, the cumulant transform for both the advected and hydrodynamic field is the same and follows the rules described in [13]. Generally, one can think of cumulants as of intensive and statistically independent quantities as opposed to (central) moments, being extensive ones. In case of the hydrodynamic field, the first order moment correspond to momentum,  $\rho\mathbf{u}$ , as opposed to first order cumulant which is just the velocity,  $\mathbf{u}$ .

### 2.1.1. Considered collision kernels

In the following subsection, four different collision kernels being investigated in the present study will be described. In all cases, the hydrodynamics collision operator  $\Omega_F$  is always based on cumulant transform  $\mathcal{C}$  and follows the formulas described in [13]. Denoting cumulants as  $\mathbf{C}^G = \mathcal{C}(\mathbf{g})$ , the cumulant collision kernel can be written as,

$$\Omega_F(\mathbf{f}) = \mathcal{C}^{-1} \left( \mathbf{C}^F + \mathbb{S}^F \left( \mathbf{C}^{F,eq} - \mathbf{C}^F \right) \right) \quad (18)$$

On the other hand, different kernels are used for the internal energy field, based on either central moments or cumulants,

$$\Omega_H(\mathbf{h}) = \mathbb{M}^{-1} \mathbb{N}^{-1} \left( \tilde{\mathbf{Y}}^H + \mathbb{S}^H \left( \tilde{\mathbf{Y}}^{H,eq} - \tilde{\mathbf{Y}}^H \right) \right), \quad (19)$$

or

$$\Omega_H(\mathbf{h}) = \mathcal{C}^{-1} \left( \mathbf{C}^H + \mathbb{S}^H \left( \mathbf{C}^{H,eq} - \mathbf{C}^H \right) \right), \quad (20)$$

The analytical form of the Maxwell-Boltzmann equilibrium distribution is used to calculate the central moments for the internal energy field (see [Appendix A](#)). The non-zero elements of equilibrium vector for  $\mathbf{h}^{eq}$  are,

$$\begin{aligned} \tilde{\mathbf{Y}}^{H,eq} &= \left[ \Upsilon_{000}^{eq}, \dots, 0, \dots, \Upsilon_{200}^{eq}, \Upsilon_{020}^{eq}, \Upsilon_{002}^{eq}, \dots, 0, \dots, \Upsilon_{220}^{eq}, \Upsilon_{202}^{eq}, \Upsilon_{022}^{eq}, \dots, 0, \dots, \Upsilon_{222}^{eq} \right]^T \\ &= \left[ H, \dots, 0, \dots, Hc_s^2, Hc_s^2, Hc_s^2, \dots, 0, \dots, Hc_s^4, Hc_s^4, Hc_s^4, \dots, 0, \dots, Hc_s^6 \right]^T. \end{aligned} \quad (21)$$

In case of cumulants, the collision kernel which has been originally implemented for the hydrodynamic field [13] requires adjustments to reflect the macroscopic advection-diffusion equation. Since the first and second-order cumulants corresponds to the mean and variance of the distribu-

tion, the equilibrium cumulants in case of an advected field read,

$$\begin{aligned} \mathbf{C}^{\text{H,eq}} &= \left[ c_{000}^{\text{eq}}, c_{100}^{\text{eq}}, c_{010}^{\text{eq}}, c_{001}^{\text{eq}}, c_{110}^{\text{eq}}, c_{101}^{\text{eq}}, c_{011}^{\text{eq}}, c_{200}^{\text{eq}}, c_{020}^{\text{eq}}, c_{002}^{\text{eq}}, \dots, c_{ijk}^{\text{eq}}, \dots, c_{122}^{\text{eq}}, c_{212}^{\text{eq}}, c_{221}^{\text{eq}}, c_{222}^{\text{eq}} \right]^\top \\ &= \left[ H, u_x, u_y, u_z, 0, 0, 0, c_s^2, c_s^2, c_s^2, \dots, 0, 0, 0, 0 \right]^\top, \end{aligned} \quad (22)$$

where  $c_s$  refers to the lattice speed of sound and is set to  $\sqrt{1/3}$ .

In the present study, a diagonal relaxation matrix is used for the advection-diffusion equation and can be formulated in a general form as,

$$\mathbb{S}^{\text{H}} = \text{diag} \left( [s_{000}, s_{100}, s_{010}, s_{001}, s_{110}, \dots, s_{ijk}, \dots, s_{222}] \right), \quad (23)$$

where three-indexes  $ijk$  correspond to the choice of moment three-indexes. The main relaxation frequency,  $s^{\text{H}}$ , corresponds to the macroscopic thermal conductivity [7]. As the density fluctuations are negligible ( $\ll 0.01\%$ ) for the cases being investigated, the main relaxation frequency can be expressed as [81]:

$$s^{\text{H}} = \frac{1}{\frac{k}{c_s^2 \delta t} + 1/2}. \quad (24)$$

Based on this framework, four collision operators are formulated. Three of them use the central moment transform and different choices of relaxation frequencies  $s_{ijk}$ , and one uses the cumulant transform.

**CM-SRT** is obtained by setting  $s_{ijk} = s^{\text{H}}$ . Thanks to  $\mathbb{S}^{\text{H}}$  being diagonal, the CM-SRT relaxation scheme is equivalent to the well known single relaxation time (SRT) scheme in the space of distribution functions,

$$\begin{aligned} \mathbf{h}^\star(\mathbf{x}, t) &= \mathbb{M}^{-1} \mathbb{N}^{-1} \tilde{\mathbf{Y}}^{\text{H},\star}(\mathbf{x}, t) \\ &= \mathbb{M}^{-1} \mathbb{N}^{-1} \left[ (\mathbb{1} - \mathbb{S}^{\text{H}}) \mathbb{N} \mathbb{M} \mathbf{h} + \mathbb{S}^{\text{H}} \tilde{\mathbf{Y}}^{\text{H,eq}} \right] \\ &= (1 - s^{\text{H}}) \mathbf{h} + \underbrace{\mathbb{1} s^{\text{H}}}_{\mathbb{S}^{\text{H}}} \underbrace{\mathbb{M}^{-1} \mathbb{N}^{-1} \tilde{\mathbf{Y}}^{\text{H,eq}}}_{\mathbf{h}^{\text{eq}}} \\ &= (1 - s^{\text{H}}) \mathbf{h} + s^{\text{H}} \mathbf{h}^{\text{eq}}. \end{aligned} \quad (25)$$

**CM-1<sup>st</sup>** is the basic approach for (central) moment based scheme for advection diffusion equation. Only the first order moments are relaxed ( $s_{ijk} = s^{\text{H}}$  for  $i + j + k = 1$ ), while the higher order central moments are set to equilibrium ( $s_{ijk} = 1$  for  $i + j + k > 1$ ). Similar relaxation approach has been adopted in [61, 62], although it has been presented in a generalized framework, indicating that the remaining relaxation rates can be tuned independently to influence numerical stability. Benchmarks conducted in the current study confirm, that the relaxation rates responsible for the higher order moments must be adjusted to mitigate *wiggles* occurring at numerically low conductivities.

**CM-TRT** origins from the two relaxation time (TRT) scheme which has been derived by Ginzburg in 2005 [10, 85], and extended in the subsequent years [86–89]. The basic idea is to separate the relaxation rate of the odd and even moments. Usually, the specific combination of the relaxation rates, known as a *magic parameter* is kept constant. As a result, the stationary, non-dimensional solution of NS or ADE is exactly controlled by the similarity numbers [89].

One of the beneficial consequences is that the transport coefficients (like viscosity, conductivity) shall not influence the apparent location of the boundary condition [71, 86]. It has been shown in [22, 80] that the TRT allows to eliminate an unphysical numerical diffusion in solid-liquid phase change model. However, the authors of the current study decided to not set the *magic parameter* for the following reasons:

- (a) The central moments' relaxation scheme does not collapse to the TRT defined in the space of distribution functions (see Appendix B).
- (b) The second order boundary conditions based on the linear interpolation schemes [56, 60] (see Section 3), which have been used in the current study do not preserve the effect of the magic parameter [90, 91]. According to [86, 92], application of *magic* boundary schemes allows to obtain viscosity independent permeability, however such extension is beyond the scope of the present work.
- (c) There is no universal, most accurate magic number [58].

In this contribution, the odd-moments are relaxed with a common rate ( $s_{odd} = s^H$ ), while the even moments are set to equilibrium ( $s_{even} = 1$ ). For further discussion regarding the relation with the original TRT model, the interested reader is referred to Appendix B.

**Cumulants-1<sup>st</sup>** follows the statistical independence of cumulants, thus only the first order cumulants are relaxed with  $s_{ijk} = s^H$  (for  $i + j + k = 1$ ), while the higher order ones are set to equilibrium values ( $s_{ijk} = 1$  for  $i + j + k > 1$ ).

### 3. Boundary Conditions (BC)

This section briefly describes the boundary conditions used within the current work. The simple bounce-back (BB) rule reduces the convergence of the LBM to first order if the wall is not located exactly between lattice nodes. The higher-order boundary condition are implemented in the present study to circumvent this issue and recover the second order convergence.

Bouzidi et al. [56] proposed the interpolated-bounce-back (IBB) scheme to represent a non-slip wall on a curved boundary. It is assumed that during each streaming step, the distributions travels a distance  $|e_i|\Delta t$ . The walls are modelled by a bounce back of said distributions back into the domain. As the wall is not necessarily half-way between lattice nodes, the algorithm employs a linear interpolation scheme between boundary node  $\mathbf{x}_b$  and neighbouring fluid node  $\mathbf{x}_f$ ,

$$f_{\bar{\alpha}}(\mathbf{x}_b, t + \Delta t) = \begin{cases} 2qf_{\alpha}^*(\mathbf{x}_b, t) + (1 - 2q)f_{\alpha}^*(\mathbf{x}_f, t) & \text{for } q \in [0, 0.5] \\ \frac{1}{2q} [f_{\alpha}^*(\mathbf{x}_b, t) + (2q - 1)f_{\alpha}^*(\mathbf{x}_b, t)] & \text{for } q \in (0.5, 1], \end{cases} \quad (26)$$

where  $q$  is the distance (along lattice link) between the boundary node and the actual boundary and  $\bar{\alpha}$  denotes direction opposite to  $\alpha$ . The idea is depicted in Fig. 1.

The interpolation scheme proposed by Bouzidi et al. [56] can be modified [57–60] to obtain Dirichlet boundary conditions for advection-diffusion problems. Due to change in sign of the post-collision distribution function, the scheme is refereed as interpolated-anti-bounce-back

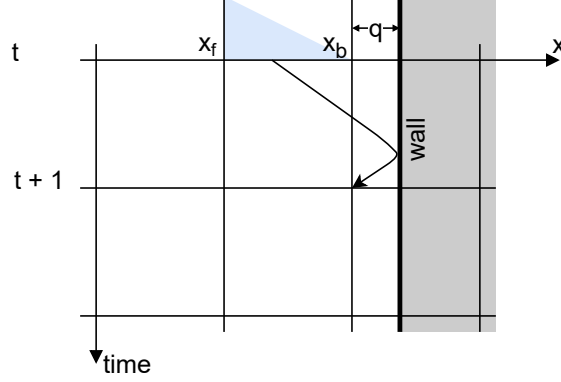


Fig. 1: Interpolated (Anti-)Bounce Back in the time-space diagram. The blue triangle indicates the intensity of the interpolation function between  $g_i^*(\mathbf{x}_b, t)$  and  $g_i^*(\mathbf{x}_f, t)$  for  $q \in [0, 0.5]$ .

(IABB),

$$h_i(\mathbf{x}_b, t + \Delta t) = \begin{cases} -[2qh_i^*(\mathbf{x}_b, t) + (1 - 2q)h_i^*(\mathbf{x}_f, t)] + 2h_i^{eq}(\mathbf{x}_w, \mathbf{u}, t) & \text{for } q \in [0, 0.5] \\ \frac{1}{2q}[-h_i^*(\mathbf{x}_b, t) + (2q - 1)h_i^*(\mathbf{x}_f, t) + 2h_i^{eq}(\mathbf{x}_w, \mathbf{u}, t)] & \text{for } q \in (0.5, 1], \end{cases} \quad (27)$$

where  $h_i^{eq}(\mathbf{x}_w, \mathbf{u}, t)$  is a source term designed to impose the desired temperature at the wall,  $\mathbf{x}_w$ . If the interpolation is skipped, then the scheme simplifies to the so called anti-bounce-back (ABB) [86, 93, 94]. In the simplest form of the Dirichlet boundary condition, known as the equilibrium scheme (EQ) [95–97], only the equilibrium part of the above equation is prescribed to the outgoing distributions.

#### 4. Model Verification and Validation

In this section, a set of numerical experiments used to evaluate the accuracy of the investigated kernels is described. The benchmarks starts with advection-diffusion problems in a fixed, external velocity field. Next, the second order boundary conditions are tested. Finally, a comprehensive study of a flow with forced convection is performed.

To assure consistency all cases are calculated with the same 3D code. In the 2D cases, the z-direction is periodic and it is cut to three elements. This is technical minimum in our solver [98, 99], because a message passing layer is used for domain decomposition. In such a setup, the 3D model reduce itself to 2D one (of course, with a higher computational cost). Observe, that the LBM weights of D3Q27 lattice, when summed over the z-direction, give the standard LBM weights for D2Q9.

The normalized  $L_2$  norm of error is utilised to compare the results between the simulations.

It is defined as,

$$L_2 = \sqrt{\frac{\sum_i (T_i^{\text{analytical}} - T_i^{\text{numerical}})^2}{\sum_i (T_i^{\text{analytical}})^2}} \quad (28)$$

where the sum  $\sum_i$  goes over all lattice nodes and  $T_i$  is the temperature in the  $i$ -th node.

#### 4.1. Advection-Diffusion of a Gaussian hill

To avoid the influence of boundary conditions, the first benchmark investigates behaviour of the collision kernels in a periodic domain. In the case of an isotropic diffusion, and convection with constant velocity, the analytical solution describing the evolution of a Gaussian hill can be derived [6, 45, 100]. The formula can be expressed as,

$$C(\mathbf{x}, t) = \frac{(2\pi\sigma_0^2)^{N/2}}{(2\pi(\sigma_0^2 + 2kt))^{N/2}} C_0 \exp\left(-\frac{(\mathbf{x} - \mathbf{x}_0 - \mathbf{u}t)^2}{2(\sigma_0^2 + 2kt)}\right) \quad (29)$$

where  $N$  is the number of spatial dimensions,  $t$  is time and  $\sigma_0$  represents the initial variance of the distribution.

Given the initial condition, the same physical case (defined by physical time,  $t_{SI}$ , physical length,  $L_{SI}$ , and physical conductivity  $k_{SI}$ ), can be simulated numerically using different time steps  $\delta t = (\delta x)^2 k_{LB} / k_{SI}$ . The  $\delta x$  denotes ratio of the physical length to the number of lattice nodes and has been fixed as  $\delta x = L_{SI} / L = 1$ . Since  $t_{SI} = n\delta t$ , where  $n$  is the number of iterations, the  $k_{LB}$  can be expressed as  $k_{LB} = (t_{SI} k_{SI}) / (n(\delta x)^2)$ . The domain was a square,  $256 \times 256 \times 3$ , with periodic boundaries. Each case has been initialised with a 2D Gaussian distribution, according to Eq. (29), with initial variance,  $\sigma_0 = 100$ . The simulations were executed for  $n$  iterations, ranging from 2400 (corresponding to  $k_{LB} = 1/6$ ) to  $40 \times 10^6$  ( $k_{LB} = 10^{-5}$ ). Once the simulation reached the prescribed number of iterations, the result was compared against the analytical solution. The  $L_2$  error norm has been plotted in Fig. 2 for each of the investigated kernels. For pure diffusion, the error of all collision kernels is small and of similar level, for  $k$

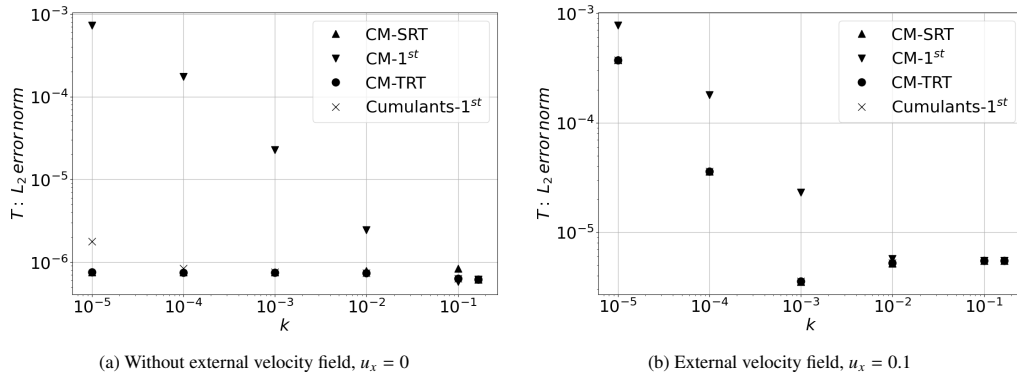


Fig. 2: Advection-diffusion of a Gaussian hill has been calculated analytically for the physical time  $t_{SI} = 100$  and physical conductivity  $k_{SI} = 4$ . To benchmark the investigated collision kernels, the same physical case has been simulated using different numerical conductivities  $k$  on a  $256 \times 256 \times 3$  lattice.

ranging from  $1/6$  to  $10^{-4}$  (see Figure 2a), except for CM-1<sup>st</sup> model, for which the error strongly depends on  $k$ . In the case of constant velocity  $\mathbf{u} = [1, 0]$ , the error of all collision kernels depend on  $k$ , as artefacts resulting from numerical dispersion dominates the ones related to diffusion (see Figure 2b). The geometrical structure of errors (*wiggles*) caused by the numerical dispersion is shown in Section 4.2.

To show the behaviour of the investigated kernels in 3D, and the geometry of the introduced error, a spherical Gaussian hill was investigated on a D3Q<sub>F</sub>27Q<sub>H</sub>27 lattice. The domain has initialised according to Eq. (29) with initial variance of  $\sigma_0^2 = 100$ . The domain was a box,  $256 \times 256 \times 256$ , with periodic boundary conditions. Conductivity of the stationary medium has been set to moderate value, namely  $k_{LB} = 10^{-3}$  and the simulation was run for  $n = 400000$  iterations. Again, the results were compared with analytical solution. All the collision kernels resulted in

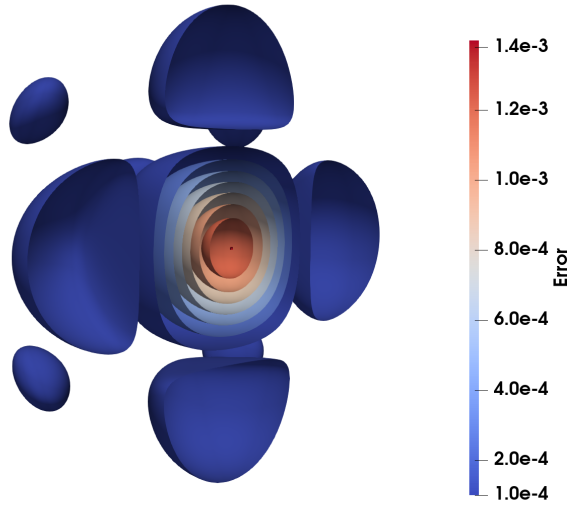


Fig. 3: The iso-contours of the absolute error of the 3D Gaussian hill for the CM-1<sup>st</sup> kernel. The simulation has been run for 400000 iterations with conductivity being set to  $k_{LB} = 10^{-3}$ .

error with spherical symmetry, except for the CM-1<sup>st</sup> kernel. The geometrical structure of the absolute error for this collision operator is shown Fig. 3. It is immediately evident that when only first-order central moments are relaxed, a considerable amount of spurious, mesh aligned, structures arise. Contrastingly, the other collision operators provided nearly identical results, with spherical symmetry and an order of magnitude smaller maximum errors, compared to CM-1<sup>st</sup>.

#### 4.2. Advection-diffusion of a square indicator function

To depict the character of wiggles caused by both external velocity field and a jump in the value of a scalar field, a simple advection-diffusion study with uniform velocity field and periodic boundary conditions has been done. The qualitative results are presented in Table 2. The dimensions of the domain were  $128 \times 128 \times 3$  [lu]. In the middle of the domain, a  $48 \times 48 \times 3$  square has been initialised with  $T = 11$ , while  $T_0 = 10$ . The conductivity has been set to  $10^{-5}$ .

Each simulation has been run for 12 800 iterations. To store the scalar field, the D3Q<sub>H</sub>7 lattice has been benchmarked against D3Q<sub>H</sub>27. It is easy to observe that the D3Q7 lattice is a subset of D3Q27. It can be obtained by limiting the set of discrete velocities,  $\mathbf{e}$ , to its first seven elements. Only the first seven central moments can be represented: the zeroth, first and second order, non-diagonal ones. As a consequence, it is not possible to distinguish between CM-1<sup>st</sup> and CM-TRT. The shape of the square advected on this lattice is distorted and strong wiggles are evident.

For the D3Q<sub>H</sub>27 lattice, all four collision kernels were compared. The CM-1<sup>st</sup> and Cumulants-1<sup>st</sup> kernels generates diffusive artefacts that appears at the corners of the resting square. The issue can be alleviated using the CM-SRT or CM-TRT kernel, which relax the higher-order moments.

#### 4.3. Heat conduction between two concentric cylinders

To asses the accuracy of a curved boundary representation, steady state heat conduction between two concentric cylinders (without flow) is studied. The geometry is shown in Fig. 4.

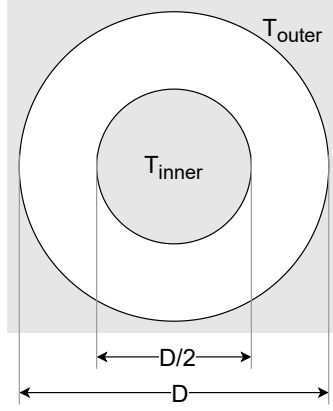


Fig. 4: The inner cylinder was a heater with diameter  $\frac{1}{2}D$ , while the outer one with diameter  $D$  was a cooler.

Heat conduction in the cylindrical coordinate system can be described by a partial differential equation,

$$\rho c_v \frac{\partial}{\partial t} T = \frac{1}{r} \frac{\partial}{\partial r} \left( k r \frac{\partial T}{\partial r} \right) + \frac{1}{r^2} \frac{\partial}{\partial \phi} \left( k \frac{\partial T}{\partial \phi} \right) + \frac{\partial}{\partial z} \left( k \frac{\partial T}{\partial z} \right) + \dot{q}. \quad (30)$$

The general solution for a 2D, steady-state case is,

$$T(r) = \frac{\lambda_1}{k} \ln \left( \frac{r}{r_{inner}} \right) + \lambda_2. \quad (31)$$

Applying the Dirichlet boundary condition for  $T(r_{inner}) = T_{inner}$  and  $T(r_{outer}) = T_{outer}$ , the unknown coefficients,  $\lambda_1, \lambda_2$  are find and the solution reads,

$$T(r) = (T_{outer} - T_{inner}) \frac{\ln \left( \frac{r}{r_{inner}} \right)}{\ln \left( \frac{r_{outer}}{r_{inner}} \right)} + T_{inner}. \quad (32)$$

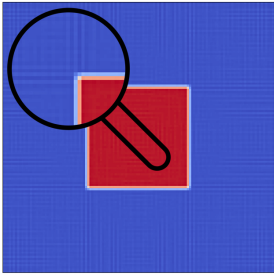
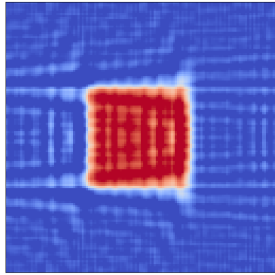
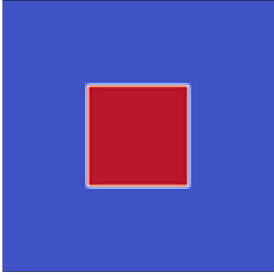
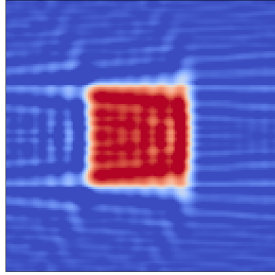
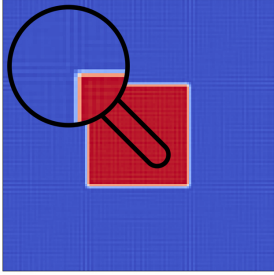
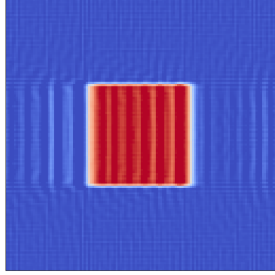
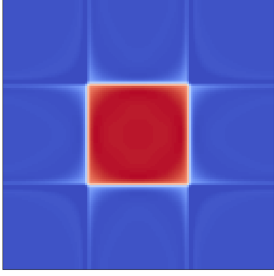
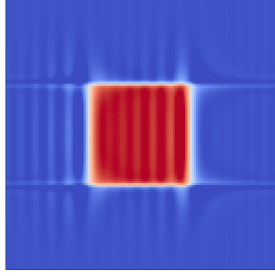
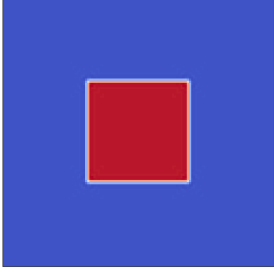
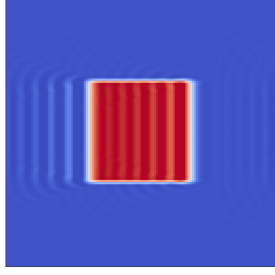
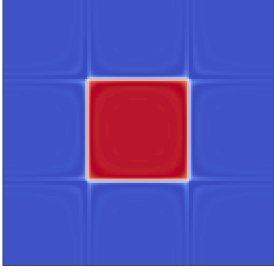
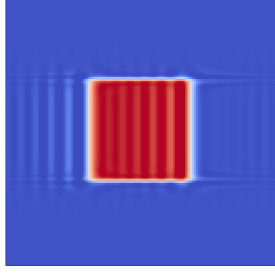
|         |                                   |   |  |
|---------|-----------------------------------|---|--|
| D3Q7    | CM-SRT                            |    |    |
|         | CM-1 <sup>st</sup> same as CM-TRT |    |    |
| D3Q27   | CM-SRT                            |   |   |
|         | CM-1 <sup>st</sup>                |  |  |
|         | CM-TRT                            |  |  |
|         | Cumulants-1 <sup>st</sup>         |  |  |
| Lattice | Kernel                            | $u = \mathbf{0}$  | $u_x = 0.1$  |

Table 2: The square has been initialised with  $T = 11$ , while  $T_0 = 10$ . The color map on all images has been clipped to range  $T \in (9.98 - 11.02)$ . The region inside the loupe has been magnified by 175%. Notice the onset of numerical noise in the background when the CM-SRT kernel is used.



In Fig. 5, three different implementations of Dirichlet's boundary condition for the internal energy field have been assessed in a circular geometry. As expected, only the IABB exhibited the second order convergence rate.

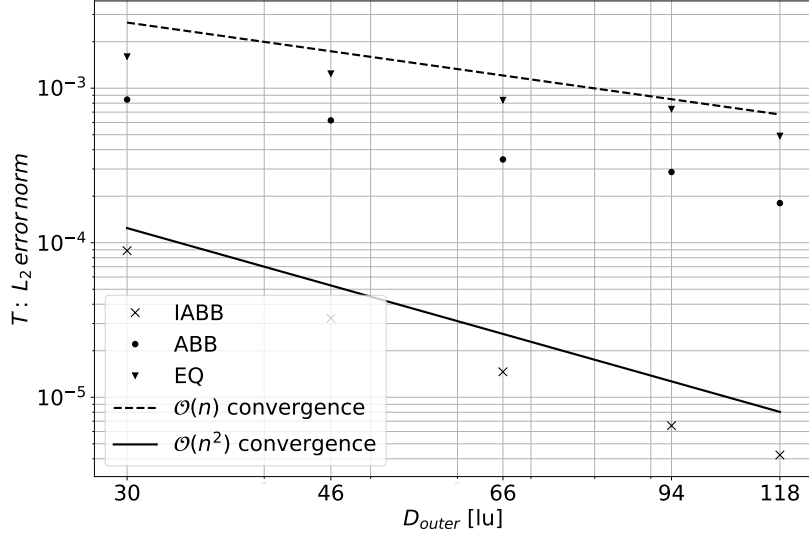


Fig. 5: Grid convergence study for the Dirichlet boundary condition. The CM-TRT collision Kernel has been used and the conductivity was set to  $k = 0.1$ . Three different implementations of boundary conditions were benchmarked. The abbreviations reads: interpolated-anti-bounce-back (IABB), anti-bounce-back (ABB), equilibrium scheme (EQ).

#### 4.4. Steady, forced convective heat transfer from a confined cylinder

From an engineering perspective, the temperature of the fluid is usually controlled by a presence of a heat exchanger. Here, a mesh dependence study of a steady forced convection from a confined cylinder is performed to illustrate the effect of the various implementation of the boundary conditions, collision kernels at different Prandtl number ( $Pr$ ) numbers. Fig. 6 presents parametrisation of the domain. All simulations have been performed on a  $D3Q_F27Q_H27$  lattice.

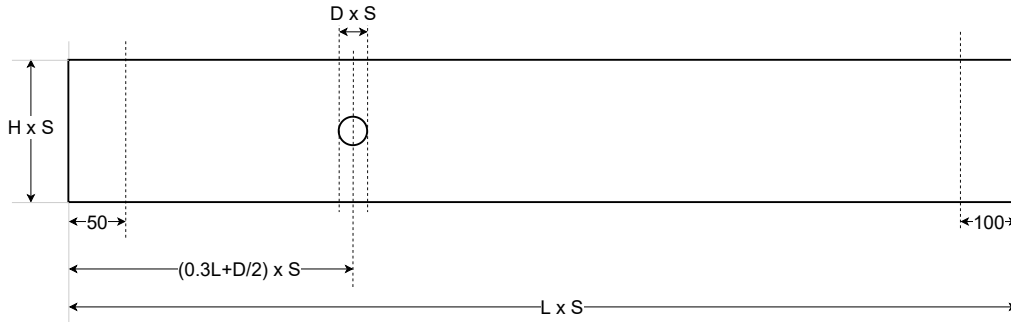


Fig. 6: Channel with hot cylinder and cross-sections used for the heat flux measurements.

To refine the lattice, a geometry scaling factor has been defined as  $S \in \{1, 2, 4\}$ . The height, length

and cylinder's diameter of the *coarse* ( $S = 1$ ) lattice are  $H = 150$  [lu],  $L = 1000$  [lu] and  $D = 30$  [lu] respectively. On the inlet, the *Zou-He* [101] BC also known as *non equilibrium bounce-back* method, with  $T_{inlet} = 10$ , has been imposed. The Neumann BC has been placed at the outlet as described in [102]. Top and bottom of the domain utilised symmetry BC. The Dirichlet BC has been prescribed on walls of the cylinder,  $T_{cylinder} = 11$ , using either first or second order implementation. In case of the first order BC, the bounce-back (BB) rule for hydrodynamics and equilibrium scheme (EQ) for internal energy field has been used. For the second order BC, the interpolated-bounce-back (IBB) and interpolated-anti-bounce-back (IABB), as described in Section 3 were employed. The LBM simulation has been iterated until heat flux calculated through the heater's surface,  $\dot{q}_{surface}$ , matched the outflow flux,  $\dot{q}_x = \dot{q}_x^{inlet} - \dot{q}_x^{outlet}$ , or the iterations limit has been reached. The heat flux through the heater's surface has been calculated as,

$$\dot{q}_{surface} = q_{out} - q_{in} = \sum_{\alpha} h_{\alpha}^* - \sum_{\alpha} h_{\alpha}, \quad (33)$$

while the heat flux through a section as,

$$\dot{q}_x^{section} = \int \rho c_v T \mathbf{u} \cdot \mathbf{n} dA = \sum_{\alpha} e_{\alpha}^x h_{\alpha}. \quad (34)$$

To limit the effect of a boundary condition, the heat flux measurements' sections for the inlet and outlet have been defined 50 and 100 [lu] away from the boundary (see Fig. 6).

The flow around a hot cylinder can be defined by two dimensionless numbers, namely Reynolds number ( $Re$ ) and Prandtl number ( $Pr$ ). The well known  $Re$  describes the ratio of inertia to viscous forces within the fluid,  $Re = \frac{uD}{\nu}$ . Subsequently, the  $Pr$  describes the relative thickness of the momentum to thermal boundary layer,  $Pr = \frac{\nu}{\alpha} = \frac{\nu \rho c_v}{k}$ . As mentioned in the Section 1, it can be also viewed as a property of a medium, which describes the ratio of time scales at which physical phenomena related to hydrodynamic and thermal field occurs. For fluids characterised by high  $Pr$  (e.g. oil), the heat diffuses much slower than the momentum and the thermal boundary layer is contained within the velocity boundary layer. In the case of liquid metals, the opposite happens. The  $Pr$  is low, heat diffuses much faster than momentum, and the velocity boundary layer is fully contained within the thermal boundary layer. Finally, the Nusselt number ( $Nu$ ) has been chosen to assess quality of the simulations. It represents the enhancement of heat transfer through a fluid as a result of convection relative to conduction across the same fluid layer. It is defined as  $Nu = \frac{\zeta D}{k}$ , where  $\zeta$  is the average convective heat transfer coefficient,  $\zeta = \dot{q}/(A(T_{cylinder} - T_{inlet}))$  and  $A = \pi D$  is the area of the cylinder. The heat flux,  $\dot{q}$ , is calculated as an average of  $\dot{q}_{surface}$  and  $\dot{q}_x^{section}$ .

In the numerical study, 72 LBM simulations were performed. The resulting  $Nu$  are compared against a high-quality solution obtained with Bubnov-Galerkin FEM solver from QuickSim CFD Toolbox for MATLAB. The FEM structural mesh consisted of 392704 second order triangular elements. Fig. 7 presents discretization of the domain behind the cylinder.

Four collision kernels were tested with first and second order BC for  $Pr \in \{10, 100, 1000\}$ . To lower the computational effort, the Reynolds number was set to 10 thus, the flow pattern could be assumed to be two-dimensional. As a consequence, the result obtained on the D3Q<sub>F</sub>27Q<sub>H</sub>27 lattice would correspond to the one obtained on D2Q<sub>F</sub>9Q<sub>H</sub>9. The coarse lattice  $1000 \times 150 \times 3$  was refined two times resulting in a medium  $2000 \times 300 \times 3$  and a fine  $4000 \times 600 \times 3$  one. The Table 3, defines the Case-ID using lattice size, input parameters. It is followed by Table 4, which

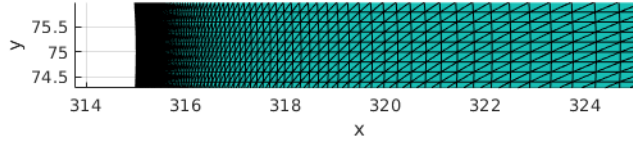


Fig. 7: The FEM mesh in the vicinity of the cylinder.

presents the outcomes for each combination of the kernel, boundary conditions and Case-ID.

| mesh   | $Pr$ | Lattice size | $D$ | $U$    | $Re$ | $\nu$              | $k$                |
|--------|------|--------------|-----|--------|------|--------------------|--------------------|
| coarse | 10   | 1000×150×3   | 30  | 0.01   | 10   | $3 \times 10^{-2}$ | $3 \times 10^{-3}$ |
| medium | 10   | 2000×300×3   | 60  | 0.005  | 10   | $3 \times 10^{-2}$ | $3 \times 10^{-3}$ |
| fine   | 10   | 4000×600×3   | 120 | 0.0025 | 10   | $3 \times 10^{-2}$ | $3 \times 10^{-3}$ |
| coarse | 100  | 1000×150×3   | 30  | 0.01   | 10   | $3 \times 10^{-2}$ | $3 \times 10^{-4}$ |
| medium | 100  | 2000×300×3   | 60  | 0.005  | 10   | $3 \times 10^{-2}$ | $3 \times 10^{-4}$ |
| fine   | 100  | 4000×600×3   | 120 | 0.0025 | 10   | $3 \times 10^{-2}$ | $3 \times 10^{-4}$ |
| coarse | 1000 | 1000×150×3   | 30  | 0.01   | 10   | $3 \times 10^{-2}$ | $3 \times 10^{-5}$ |
| medium | 1000 | 2000×300×3   | 60  | 0.005  | 10   | $3 \times 10^{-2}$ | $3 \times 10^{-5}$ |
| fine   | 1000 | 4000×600×3   | 120 | 0.0025 | 10   | $3 \times 10^{-2}$ | $3 \times 10^{-5}$ |

Table 3: The summary of executed cases. The variables,  $D$ ,  $U$ ,  $\nu$  and  $k$  are expressed in lattice units.

As far as the numerical conductivity is relatively high ( $k = 3 \times 10^{-3}$ ), all kernels provided good results even with first order BC on each lattice. Once the conductivity is lowered by order of magnitude, ( $k = 3 \times 10^{-4}$ ), discrepancies occur for the CM-1<sup>st</sup> and Cumulants-1<sup>st</sup> kernel on the coarse lattice. The mismatching results origin from relaxing first-order central moments or cumulants with frequencies corresponding to thermal conductivity, while higher-order quantities were relaxed towards equilibrium. Although benefits from the second-order boundary conditions can be clearly observed, they are not sufficient to counterweight the aforementioned effect. For the most numerically challenging case ( $k = 3 \times 10^{-5}$ ), the CM-TRT kernel provided results with highest quality. Interestingly, the CM-SRT kernel performed reasonably well, except the coarsest lattice for which the wiggles in the temperature field reached the inlet (Fig. 9b), causing the heat flux to be spurious. Notice that the behaviour of numerical artefacts for kernel pairs { CM-SRT, CM-TRT } and { CM-1<sup>st</sup>, Cumulants-1<sup>st</sup> } is similar. Following the imposed BC, the physical temperature range shall be contained within the values of 10 and 11. Other values are undoubtedly artefacts (see Fig. 9, in which the temperature range has been clipped to highlight the issue). In the case of second-order boundary conditions, the shape of the artefacts was preserved, but the magnitude was decreased.

## 5. Future outlook

The authors decided to skip the benchmarks involving buoyancy force (natural convection inside a heated cavity or Rayleigh-Bernard convection) to limit the number of factors which can influence the results. Readers interested in the proper treatment of the forcing term are referred to discussions in [13, 103–108].

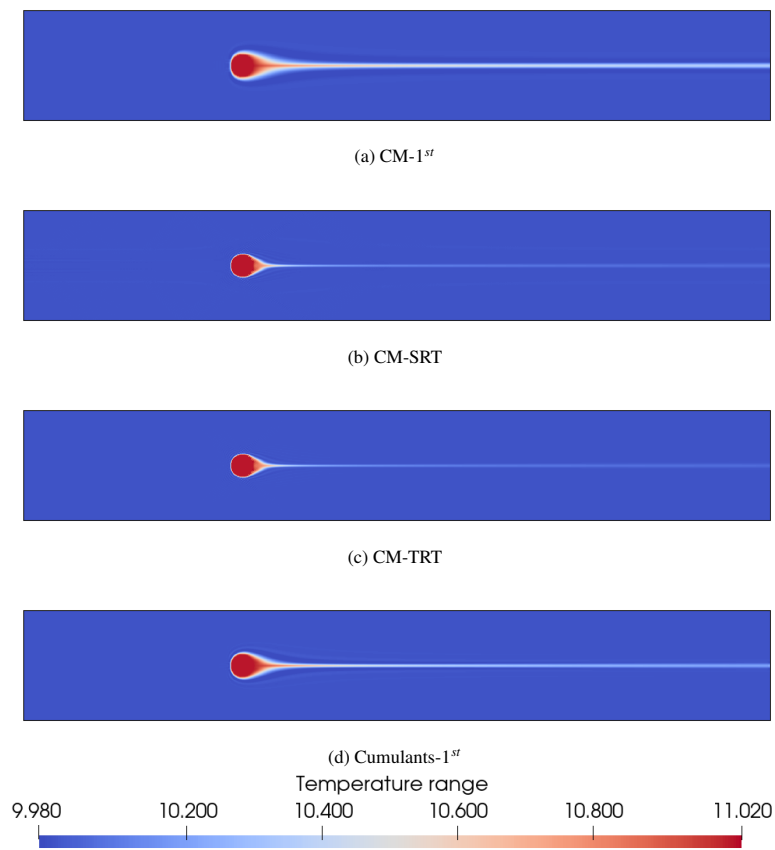


Fig. 8: The temperature field is simulated using four different collision kernels. The color scale is restricted to  $T \in [9.98, 11.02]$ . The flow is computed, on a coarse mesh:  $1000 \times 150 \times 3$ , using 1<sup>st</sup> order boundary conditions. The cylinder diameter is  $D=30$  [lu] and the inlet velocity is  $U=0.01$  [lu/ts]. The relaxation frequencies corresponds to  $\nu = 3 \times 10^{-2}$  and  $k = 3 \times 10^{-5}$  ( $Re = 10$ ,  $Pr = 1000$ ).

| mesh   | $Pr$ | CM-1 <sup>st</sup>        |                 | CM-SRT          |                 | CM-TRT          |                 | Cumulants-1 <sup>st</sup> |                 | FEM   |
|--------|------|---------------------------|-----------------|-----------------|-----------------|-----------------|-----------------|---------------------------|-----------------|-------|
|        |      | BC order: 1 <sup>st</sup> | 2 <sup>nd</sup> | 1 <sup>st</sup> | 2 <sup>nd</sup> | 1 <sup>st</sup> | 2 <sup>nd</sup> | 1 <sup>st</sup>           | 2 <sup>nd</sup> |       |
| coarse | 10   | 3.44                      | 4.91            | 4.94            | 4.81            | 4.91            | 4.81            | 5.04                      | 4.83            | 4.82  |
| medium | 10   | 5.03                      | 4.84            | 4.87            | 4.81            | 4.86            | 4.81            | 4.92                      | 4.82            | 4.82  |
| fine   | 10   | 4.92                      | 4.83            | 4.84            | 4.81            | 4.83            | 4.81            | 4.87                      | 4.81            | 4.82  |
| coarse | 100  | 20.68                     | 14.75           | 10.64           | 10.20           | 10.66           | 10.27           | 14.50                     | 11.52           | 10.10 |
| medium | 100  | 15.87                     | 11.84           | 10.33           | 10.11           | 10.32           | 10.13           | 11.82                     | 10.36           | 10.10 |
| fine   | 100  | 12.96                     | 10.64           | 10.20           | 10.09           | 10.19           | 10.08           | 10.83                     | 10.13           | 10.10 |
| coarse | 1000 | 166.42                    | 102.27          | -71.52          | -57.02          | 27.09           | 24.58           | 94.31                     | 58.33           | 21.43 |
| medium | 1000 | 111.76                    | 62.52           | 22.75           | 21.78           | 22.73           | 21.84           | 53.97                     | 34.19           | 21.43 |
| fine   | 1000 | 74.00                     | 40.47           | 21.87           | 21.38           | 21.84           | 21.37           | 34.04                     | 24.56           | 21.43 |

Table 4: The  $Nu$  number, computed for different collision kernels and boundary conditions (see Table 3). 1<sup>st</sup>order BC – BB (hydrodynamics) & EQ (thermodynamics), 2<sup>nd</sup>order BC – IBB (hydrodynamics) & IABB (thermodynamics). The FEM has been used to obtain reference solution.

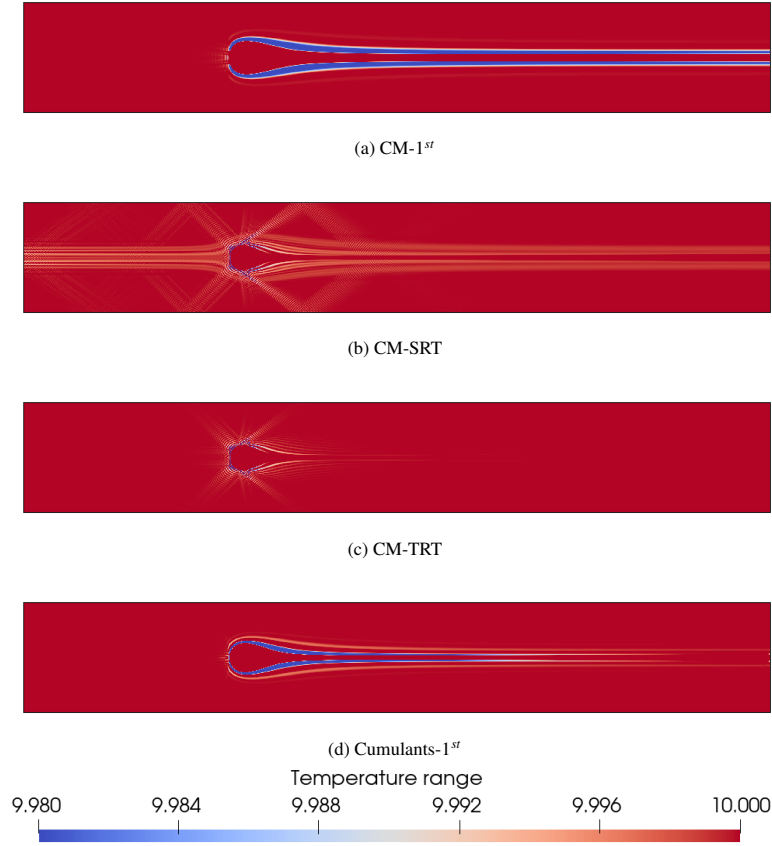


Fig. 9: The temperature field is simulated using four different collision kernels, for the same case as 8. Plotted in a color scale restricted the spurious temperature range,  $T \in [9.98, 10.00]$ , to highlight the numerical artefacts.

Although an increase of the resolution might be enough to break the necessity of a larger stencil for the investigated cases, it is not obvious whether such an approach would be computationally cheaper, especially that both lattices responsible for the hydrodynamics and the advected field must be refined.

The seek of optimal relaxation frequencies for central moments, or cumulant collision kernel responsible for the advected field deserves further study. The relationship between higher order cumulants and central moments is non-linear, thus the conclusions related to the relaxation of higher-order central moments can not be projected to cumulants in a straightforward fashion. Due to the similarity between central moments and cumulants for order lower than fourth [4, 13], one may expect improvements by relaxing third-order cumulants. However, such extension is beyond the scope of the current research. As a good starting point, research regarding parametrisation of the cumulant kernel responsible for the hydrodynamic field [14] can be recommended. In terms collision operators which can be expressed in a matrix form, a comprehensive method for recovering equivalent partial differential equations has been recently proposed by Fučík and Straka [109].

## 6. Conclusions

In this work, an analysis of the state of the art collision kernels applied to both hydrodynamic and the advected field with a focus on the relaxation of the higher-order moments has been presented. To isolate features which may affects the accuracy of the proposed kernels a set of simple benchmarks was conducted. The tests has been performed in a numerically challenging, high Prandtl number regime. To alleviate the numerical artefacts raised by low conductivity, a D3Q27 lattice has been utilized for the advected field. However, lattices with large number of discrete velocities introduce additional degrees of freedom to the relaxation scheme. We demonstrated that proper treatment of the collision kernel plays a more important role than the application of second-order boundary conditions to represent a curved geometry. To sum up, for the set of investigated benchmarks, characterized by specific grid resolution and a range of non-dimensional numbers, the beneficial effect of tuning of the relaxation coefficients corresponding to the higher order moments has been confirmed numerically and the CM-TRT followed by CM-SRT kernel has been shown to be superior to the kernels that relax only first-order central moments/cumulants.

## 7. Acknowledgements

W. Regulski, J. Szumbariski and M. Dzikowski are appreciated for insightful discussions. C. Leonardi is acknowledged for proofreading of the manuscript. The computational resources have been provided by *Rysy* cluster at Interdisciplinary Centre for Mathematical and Computational Modelling and *Prometheus* cluster at Cyfronet Computing Center belonging to PL-Grid Infrastructure. This work was partially supported by funds granted by QuickerSim Ltd. and Warsaw University of Technology, namely *Rada Naukowa Dyscypliny Inżynieria Mechaniczna*. The simulations were completed using the open-source TCLB solver [98, 99] available at: <https://github.com/CFD-GO/TCLB>

## 8. Conflict of interest

None declared.

## Appendix A. Discretisation of the equilibrium distribution function

Some authors favour the usage of the Hermite polynomials to discretise the equilibrium distribution function [74, 107]. In this section, an common alternative [9] is discussed.

The continuous Maxwell-Boltzmann distribution function is known as,

$$\Psi^{M-B, eq} = \Psi^{M-B, eq}(\psi, \boldsymbol{\xi}, \mathbf{u}) = \frac{\psi}{(2\pi c_s^2)^{N/2}} \exp\left[-\frac{(\boldsymbol{\xi} - \mathbf{u})^2}{2c_s^2}\right], \quad (\text{A.1})$$

where  $\psi$  is the quantity of interest (like density or internal energy) and  $N$  is the number of spatial dimensions. The definition of the central moments for a continuous distribution is,

$$\tilde{\Upsilon}_{mn} = \int_{-\infty}^{\infty} \int_{-\infty}^{\infty} (\xi_x - u_x)^m (\xi_y - u_y)^n \Psi(\psi, \boldsymbol{\xi}, \mathbf{u}) d\xi_x d\xi_y. \quad (\text{A.2})$$

To illustrate the analysis with a relatively short example, a D2Q9 lattice with the following order of the central moments is investigated,

$$\tilde{\Upsilon} = [\tilde{\Upsilon}_{00}, \tilde{\Upsilon}_{10}, \tilde{\Upsilon}_{01}, \tilde{\Upsilon}_{20}, \tilde{\Upsilon}_{02}, \tilde{\Upsilon}_{11}, \tilde{\Upsilon}_{21}, \tilde{\Upsilon}_{12}, \tilde{\Upsilon}_{22}]^T. \quad (\text{A.3})$$

The resulting moments and central moments for the internal energy (with  $\psi = H = \Upsilon_{00}^H = \rho c_v T$ ) are,

$$\Upsilon^{H, eq} = \Upsilon_{00}^H \begin{bmatrix} 1 \\ u_x \\ u_y \\ (u_x^2 + c_s^2) \\ (u_y^2 + c_s^2) \\ u_x u_y \\ u_y (u_x^2 + c_s^2) \\ u_x (u_y^2 + c_s^2) \\ (u_x^2 u_y^2 + c_s^2 u_x^2 + c_s^2 u_y^2 + c_s^4) \end{bmatrix}, \quad (\text{A.4})$$

$$\tilde{\Upsilon}^{H, eq} = \Upsilon_{00}^H \begin{bmatrix} 1 \\ 0 \\ 0 \\ c_s^2 \\ c_s^2 \\ 0 \\ 0 \\ 0 \\ c_s^4 \end{bmatrix}. \quad (\text{A.5})$$

In general, the central moments of a physical quantity being in equilibrium should be independent of the velocity. Next, the discrete equilibrium distribution can be obtained using backward transformation from central moments space,

$$\mathbf{h}^{eq} = \mathbb{M}^{-1} \mathbb{N}^{-1} \tilde{\Upsilon}^{H, eq}, \quad (\text{A.6})$$

and the result is the same as in case of full order Hermite expansion [74, 107].

## Appendix B. Two Relaxation Time

To show the origin of the even and odd moments, consider decomposition of the discrete distribution function into symmetric (even) and anti-symmetric (odd) part:

$$\begin{aligned} h_\alpha^s &= \frac{h_\alpha + h_{\bar{\alpha}}}{2}, \\ h_\alpha^a &= \frac{h_\alpha - h_{\bar{\alpha}}}{2}. \end{aligned}$$

The discrete equilibrium distribution is treated analogously,

$$\begin{aligned} h_\alpha^{seq} &= \frac{h_\alpha^{eq} + h_{\bar{\alpha}}^{eq}}{2}, \\ h_\alpha^{aeq} &= \frac{h_\alpha^{eq} - h_{\bar{\alpha}}^{eq}}{2}. \end{aligned}$$

Next, the collision reads,

$$\mathbf{h}^*(\mathbf{x}, t) = \mathbf{h} + \frac{1}{\tau_s}[\mathbf{h}^{seq} - \mathbf{h}^s] + \frac{1}{\tau_a}[\mathbf{h}^{aeq} - \mathbf{h}^a]. \quad (\text{B.1})$$

Multiplying by  $\mathbb{M}$ , the scheme can be transferred to the moment space

$$\Upsilon^{H,*}(\mathbf{x}, t) = \Upsilon^H + \frac{1}{\tau_s}[\Upsilon^{H,seq} - \Upsilon^{H,s}] + \frac{1}{\tau_a}[\Upsilon^{H,aeq} - \Upsilon^{H,a}]. \quad (\text{B.2})$$

The two-relaxation time approach requires the odd-moments, to be relaxed with a common rate  $s_{odd}$ , while the even moments, with  $s_{even}$ . When the combination of odd and even relaxation rates is kept constant, then the steady state, non-dimensional solution of NS or ADE is *exactly* controlled by the similarity numbers (Reynolds number, Péclet number, etc.) [89]. The so called magic parameter has been defined as,

$$\Lambda = \left( \frac{1}{s_{odd}} - \frac{1}{2} \right) \left( \frac{1}{s_{even}} - \frac{1}{2} \right). \quad (\text{B.3})$$

It is interesting to observe, that vectors describing  $\{\Upsilon^{H,seq}, \Upsilon^{H,s}\}$  and  $\{\Upsilon^{H,a}, \Upsilon^{H,a}\}$  contain elements with zero values at the same indices (see Eqs. (B.7) and (B.8)). Moreover, the relaxation matrix  $\mathbb{S}^H$  is diagonal. As a consequence, the Eq. (B.2) can be simplified further to:

$$\begin{aligned} \Upsilon^{H,*}(\mathbf{x}, t) &= \Upsilon^H + \mathbb{S}^H(\Upsilon^{H,eq} - \Upsilon^H) \\ &= (\mathbb{1} - \mathbb{S}^H)\Upsilon^H + \mathbb{S}^H\Upsilon^{H,eq}. \end{aligned} \quad (\text{B.4})$$



The transformation to the central moments space can be performed in two ways. In the first approach, which follows the original idea of Ginzburg [10, 85], the Eq. (B.2) is multiplied by  $\mathbb{N}$ ,

$$\tilde{\Upsilon}^{H,*}(\mathbf{x}, t) = \tilde{\Upsilon}^H + \frac{1}{\tau_s}[\tilde{\Upsilon}^{H,seq} - \tilde{\Upsilon}^{H,s}] + \frac{1}{\tau_a}[\tilde{\Upsilon}^{H,aeq} - \tilde{\Upsilon}^{H,a}]. \quad (\text{B.5})$$

In the second approach, the Eq. (B.4) is transformed,

$$\begin{aligned} \tilde{\Upsilon}^{H,*}(\mathbf{x}, t) &= \tilde{\Upsilon}^H + \mathbb{S}^H(\tilde{\Upsilon}^{H,eq} - \tilde{\Upsilon}^H) \\ &= (\mathbb{1} - \mathbb{S}^H)\tilde{\Upsilon}^H + \mathbb{S}^H\tilde{\Upsilon}^{H,eq}. \end{aligned} \quad (\text{B.6})$$

As the structure of  $\{\tilde{\Upsilon}^{H,seq}, \tilde{\Upsilon}^{H,s}\}$  vectors (see Eq. (B.9)) do not contain zero elements, thus the Eq. (B.5) does not collapse to Eq. (B.6).

In this contribution, the full order, discrete equilibrium distribution function given in Eq. (A.6) is used to express  $h_i^{seq}$  and  $h_i^{aeq}$ . Their moments can be calculated using Eqs. (14) and (15),

$$\Upsilon^{H,seq} = \Upsilon_{00}^H \begin{bmatrix} 1 \\ 0 \\ 0 \\ u_x^2 + c_s^2 \\ u_y^2 + c_s^2 \\ u_x u_y \\ 0 \\ 0 \\ u_x^2 u_y^2 + c_s^2 u_x^2 + c_s^2 u_y^2 + c_s^4 \end{bmatrix}, \quad \Upsilon^{H,aeq} = \Upsilon_{00}^H \begin{bmatrix} 0 \\ u_x \\ u_y \\ 0 \\ 0 \\ 0 \\ 0 \\ u_y(u_x^2 + c_s^2) \\ u_x(u_y^2 + c_s^2) \\ 0 \end{bmatrix}. \quad (\text{B.7})$$

The moments of symmetric and anti-symmetric distribution function exhibits analogous structure,

$$\Upsilon^{H,s} = \begin{bmatrix} \Upsilon_{00}^{H,s} \\ 0 \\ 0 \\ \Upsilon_{20}^{H,s} \\ \Upsilon_{02}^{H,s} \\ \Upsilon_{11}^{H,s} \\ 0 \\ 0 \\ \Upsilon_{22}^{H,s} \end{bmatrix}, \quad \Upsilon^{H,a} = \begin{bmatrix} 0 \\ \Upsilon_{10}^{H,s} \\ \Upsilon_{01}^{H,s} \\ 0 \\ 0 \\ 0 \\ \Upsilon_{21}^{H,s} \\ \Upsilon_{12}^{H,s} \\ 0 \end{bmatrix}. \quad (\text{B.8})$$

These results extend the analysis done in [80], which was limited to raw, second-order moments and truncated (to linear and quadratic velocity terms) discrete equilibrium function. Finally, the

central moments are,

$$\tilde{\mathbf{Y}}^{H,seq} = \mathbf{Y}_{00}^H \begin{bmatrix} 1 \\ -u_x \\ -u_y \\ 2u_x^2 + c_s^2 \\ 2u_y^2 + c_s^2 \\ 2u_x u_y \\ -u_y(4u_x^2 + c_s^2) \\ -u_x(4u_y^2 + c_s^2) \\ 8u_x^2 u_y^2 + 2c_s^2(u_x^2 + u_y^2) + c_s^4 \end{bmatrix}, \quad \tilde{\mathbf{Y}}^{H,aeq} = \mathbf{Y}_{00}^H \begin{bmatrix} 0 \\ u_x \\ u_y \\ -2u_x^2 \\ -2u_y^2 \\ -2u_x u_y \\ u_y(4u_x^2 + c_s^2) \\ u_x(4u_y^2 + c_s^2) \\ -(8u_x^2 u_y^2 + 2c_s^2(u_x^2 + u_y^2)) \end{bmatrix}. \quad (\text{B.9})$$

### Appendix C. Transformation Matrices

From the computational point of view, it is preferred to perform the transformations to the central moments space in two steps, using Eqs. (16) and (17). Since  $\tilde{\mathbf{Y}} = \mathbb{T}\mathbf{g} = \mathbb{N}\mathbb{M}\mathbf{g}$ , the  $\mathbb{N}$  matrix can be found as  $\mathbb{N} = \mathbb{T}\mathbb{M}^{-1}$ . Rows of the transformation matrices are calculated analogously to  $\mathbf{Y}$  and  $\tilde{\mathbf{Y}}$ . For a D3Q27 lattice, each row consists of  $q \in \{1, 2, \dots, 27\}$  elements,

$$\mathbf{M}_{mno} = [M_{mno|1}, M_{mno|2}, \dots, M_{mno|\alpha}, \dots, M_{mno|q-1}, M_{mno|q}], \quad (\text{C.1})$$

$$\mathbf{T}_{mno} = [T_{mno|1}, T_{mno|2}, \dots, T_{mno|\alpha}, \dots, T_{mno|q-1}, T_{mno|q}]. \quad (\text{C.2})$$

The  $mno$  subscript refers to the order of moment, while  $\alpha$ -th subscript indicates the index of the element in the  $\mathbf{M}_{mno}$  row. Each element can be calculated as,

$$M_{mno|\alpha} = (e_{\alpha x})^m (e_{\alpha y})^n (e_{\alpha z})^o, \quad (\text{C.3})$$

$$T_{mno|\alpha} = (e_{\alpha x} - u_x)^m (e_{\alpha y} - u_y)^n (e_{\alpha z} - u_z)^o. \quad (\text{C.4})$$

Next, the matrices are assembled row by row as,

$$\mathbb{M} = [\mathbf{M}_{000}, \mathbf{M}_{100}, \mathbf{M}_{010}, \mathbf{M}_{001}, \mathbf{M}_{110}, \mathbf{M}_{101}, \mathbf{M}_{011}, \mathbf{M}_{200}, \mathbf{M}_{020}, \mathbf{M}_{002}, \dots, \mathbf{M}_{ijk}, \dots, \mathbf{M}_{122}, \mathbf{M}_{212}, \mathbf{M}_{221}, \mathbf{M}_{222}]^T, \\ \mathbb{T} = [\mathbf{T}_{000}, \mathbf{T}_{100}, \mathbf{T}_{010}, \mathbf{T}_{001}, \mathbf{T}_{110}, \mathbf{T}_{101}, \mathbf{T}_{011}, \mathbf{T}_{200}, \mathbf{T}_{020}, \mathbf{T}_{002}, \dots, \mathbf{T}_{ijk}, \dots, \mathbf{T}_{122}, \mathbf{T}_{212}, \mathbf{T}_{221}, \mathbf{T}_{222}]^T.$$

### Appendix D. Source term treatment

For completeness of the study, the addition of the source term to the cumulant collision kernel is described in this appendix from the theoretical point of view. It is known in the literature [6], that the integration of the discrete Boltzmann equation with trapezoidal rule leads to implicit evolution equation,

$$h_\alpha(\mathbf{x} + \mathbf{e}_\alpha \delta t, t + \delta t) = \Omega_{H,\alpha}(\mathbf{h}(\mathbf{x}, t)) + \frac{1}{2} [q_\alpha(\mathbf{x} + \mathbf{e}_\alpha \delta t, t + \delta t) + q_\alpha(\mathbf{x}, t)]. \quad (\text{D.1})$$

To remove the implicitness, a shift of variables is conducted and denoted with tilde,

$$\tilde{h}_\alpha = h_\alpha - \frac{1}{2}q_\alpha \quad (\text{D.2})$$

$$\tilde{H} = \sum_\alpha \tilde{h}_\alpha = H - \frac{1}{2}Q. \quad (\text{D.3})$$

The  $q_\alpha$  and  $Q$  denote the discretized source term and its zeroth moment respectively. A more detailed discussion of this procedure can be found in the recent work done by authors [110] and references therein.

By transforming source term to the cumulant space, where the collision is performed, the augmented form of Eq. (20) can be written as,

$$\Omega_H(\tilde{\mathbf{h}}) = \mathcal{C}^{-1} \left( \tilde{\mathcal{C}}^H + \mathbb{S}^H (\tilde{\mathcal{C}}^{\text{H,eq}} - \tilde{\mathcal{C}}^H) + (1 - \mathbb{S}^H/2) \mathcal{C}^Q \right). \quad (\text{D.4})$$

The simplicity of the source term in the cumulants space is noteworthy,

$$\begin{aligned} \mathcal{C}^Q = \mathcal{C}(Q) &= [c_{000}^Q, c_{100}^Q, c_{010}^Q, c_{001}^Q, c_{110}^Q, c_{101}^Q, c_{011}^Q, c_{200}^Q, c_{020}^Q, c_{002}^Q, \dots, c_{ijk}^{eq}, \dots, c_{122}^Q, c_{212}^Q, c_{221}^Q, c_{222}^Q]^\top \\ &= [Q, 0, 0, 0, 0, 0, 0, 0, 0, 0, \dots, 0, 0, 0, 0]^\top. \end{aligned} \quad (\text{D.5})$$

## References

- [1] H. K. Versteeg, W. Malalasekera, An introduction to computational fluid dynamics: the finite volume method, Pearson education, 2007.
- [2] O. Zienkiewicz, R. Taylor, P. Nithiarasu, The finite element method for fluid dynamics, vol. 3, Elsevier: Oxford (2005).
- [3] L. S. Luo, W. Liao, X. Chen, Y. Peng, W. Zhang, Numerics of the lattice Boltzmann method: Effects of collision models on the lattice Boltzmann simulations, Physical Review E - Statistical, Nonlinear, and Soft Matter Physics 83 (2011) 56710.
- [4] C. Coreixas, B. Chopard, J. Latt, Comprehensive comparison of collision models in the lattice Boltzmann framework: Theoretical investigations, Physical Review E 100 (2019) 033305.
- [5] C. Coreixas, G. Wissocq, B. Chopard, J. Latt, Impact of collision models on the physical properties and the stability of lattice Boltzmann methods, Philosophical Transactions of the Royal Society A: Mathematical, Physical and Engineering Sciences 378 (2020).
- [6] T. Krüger, H. Kusumaatmaja, A. Kuzmin, O. Shardt, G. Silva, E. M. Viggien, The Lattice Boltzmann Method, 2017.
- [7] S. Succi, The Lattice Boltzmann Equation For Complex States of Flowing Matter, Oxford University Press, 2019.
- [8] D. d’Humières, Generalized lattice-boltzmann equations, Rarefied gas dynamics (1992).
- [9] M. Geier, A. Greiner, J. G. Korvink, Cascaded digital lattice Boltzmann automata for high Reynolds number flow, Physical Review E - Statistical, Nonlinear, and Soft Matter Physics 73 (2006) 1–10.
- [10] I. Ginzburg, Equilibrium-type and link-type lattice Boltzmann models for generic advection and anisotropic-dispersion equation, Advances in Water Resources 28 (2005) 1171–1195.
- [11] F. Dubois, T. Février, B. Graille, On the stability of a relative velocity lattice Boltzmann scheme for compressible Navier-Stokes equations, Comptes Rendus Mécanique 343 (2015) 599–610.
- [12] D. d’Humières, Multiple-relaxation-time lattice Boltzmann models in three dimensions, Philosophical Transactions of the Royal Society of London. Series A: Mathematical, Physical and Engineering Sciences 360 (2002) 437–451.
- [13] M. Geier, M. Schonherr, A. Pasquali, M. Krafczyk, The cumulant lattice Boltzmann equation in three dimensions: Theory and validation, Computers and Mathematics with Applications 70 (2015) 507–547.
- [14] M. Geier, A. Pasquali, M. Schönher, Parametrization of the cumulant lattice Boltzmann method for fourth order accurate diffusion part I: Derivation and validation, Journal of Computational Physics 348 (2017) 862–888.

- [15] Q. Li, K. H. Luo, Q. J. Kang, Y. L. He, Q. Chen, Q. Liu, Lattice Boltzmann methods for multiphase flow and phase-change heat transfer, *Progress in Energy and Combustion Science* 52 (2016) 62–105.
- [16] X. He, S. Chen, G. D. Doolen, A Novel Thermal Model for the Lattice Boltzmann Method in Incompressible Limit, *Journal of Computational Physics* 146 (1998) 282–300.
- [17] R. Mabrouk, H. Dhahri, H. Naji, S. Hammouda, Z. Younsi, Lattice Boltzmann simulation of forced convection melting of a composite phase change material with heat dissipation through an open-ended channel, *International Journal of Heat and Mass Transfer* 153 (2020) 119606.
- [18] W. Du, S. Chen, G. Wu, A new lattice Boltzmann method for melting processes of high Prandtl number phase change materials, *Journal of Energy Storage* 41 (2021) 103006.
- [19] S. Chen, W. Li, H. I. Mohammed, Heat transfer of large Prandtl number fluids in porous media by a new lattice Boltzmann model, *International Communications in Heat and Mass Transfer* 122 (2021) 105129.
- [20] Z. Guo, C. Zheng, B. Shi, T. S. Zhao, Thermal lattice Boltzmann equation for low Mach number flows: Decoupling model, *Physical Review E - Statistical, Nonlinear, and Soft Matter Physics* 75 (2007) 1–15.
- [21] Y. Feng, P. Sagaut, W. Tao, A three dimensional lattice model for thermal compressible flow on standard lattices, *Journal of Computational Physics* 303 (2015) 514–529.
- [22] R. Huang, H. Wu, Phase interface effects in the total enthalpy-based lattice Boltzmann model for solid-liquid phase change, *Journal of Computational Physics* 294 (2015) 346–362.
- [23] Z. Li, M. Yang, Y. Zhang, Lattice Boltzmann method simulation of 3-D natural convection with double MRT model, *International Journal of Heat and Mass Transfer* 94 (2016) 222–238.
- [24] Z. Chen, C. Shu, D. Tan, A simplified thermal lattice Boltzmann method without evolution of distribution functions, *International Journal of Heat and Mass Transfer* 105 (2017) 741–757.
- [25] K. V. Sharma, R. Straka, F. W. Tavares, New Cascaded Thermal Lattice Boltzmann Method for simulations of advection-diffusion and convective heat transfer, *International Journal of Thermal Sciences* 118 (2017) 259–277.
- [26] K. V. Sharma, R. Straka, F. W. Tavares, Natural convection heat transfer modeling by the cascaded thermal lattice Boltzmann method, *International Journal of Thermal Sciences* 134 (2018) 552–564.
- [27] L. Fei, K. H. Luo, Cascaded lattice Boltzmann method for incompressible thermal flows with heat sources and general thermal boundary conditions, *Computers and Fluids* 165 (2018) 89–95.
- [28] L. Fei, K. H. Luo, Cascaded lattice Boltzmann method for thermal flows on standard lattices, *International Journal of Thermal Sciences* 132 (2018) 368–377.
- [29] J. H. Lu, H. Y. Lei, C. S. Dai, A unified thermal lattice Boltzmann equation for conjugate heat transfer problem, *International Journal of Heat and Mass Transfer* 126 (2018) 1275–1286.
- [30] N. Hosseini, S. A. A. and Darabiha, D. Thevenin, Lattice Boltzmann advection-diffusion model for conjugate heat transfer in heterogeneous media, *International Journal of Heat and Mass Transfer* 132 (2019) 906–919.
- [31] Y. L. Feng, S. L. Guo, W. Q. Tao, P. Sagaut, Regularized thermal lattice Boltzmann method for natural convection with large temperature differences, *International Journal of Heat and Mass Transfer* 125 (2018) 1379–1391.
- [32] A. Xu, L. Shi, H. D. Xi, Lattice Boltzmann simulations of three-dimensional thermal convective flows at high Rayleigh number, *International Journal of Heat and Mass Transfer* 140 (2019) 359–370.
- [33] Y. H. Yip, A. K. Soh, J. J. Foo, Flow-dynamics induced thermal management of crude oil wax melting: Lattice Boltzmann modeling, *International Journal of Thermal Sciences* 137 (2019) 675–691.
- [34] H. Sajjadi, A. Amiri Delouei, M. Sheikholeslami, M. Atashafrooz, S. Succi, Simulation of three dimensional MHD natural convection using double MRT Lattice Boltzmann method, *Physica A: Statistical Mechanics and its Applications* 515 (2019) 474–496.
- [35] X. B. Nie, X. Shan, H. Chen, Galilean invariance of lattice Boltzmann models, *EPL* 81 (2008) 34005.
- [36] X. He, S. Chen, G. D. Doolen, A Novel Thermal Model for the Lattice Boltzmann Method in Incompressible Limit, *Journal of Computational Physics* 146 (1998) 282–300.
- [37] C. Cercignani, *The Boltzmann Equation and Its Application*, Springer, 1988.
- [38] H. Chen, P. Gopalakrishnan, R. Zhang, Recovery of Galilean Invariance in Thermal Lattice Boltzmann Models for Arbitrary Prandtl Number, *International Journal of Modern Physics C* 25 (2014) 1450046.
- [39] X. Shan, Central-moment-based Galilean-invariant multiple-relaxation-time collision model, *Physical Review E* 100 (2019).
- [40] P. Lallemand, L. S. Lou, Hybrid finite-difference thermal lattice Boltzmann equation, *International Journal of Modern Physics B* 17 (2003) 41–47.
- [41] S. Saito, A. De Rosis, L. Fei, K. H. Luo, K. I. Ebihara, A. Kaneko, Y. Abe, Lattice Boltzmann modeling and simulation of forced-convection boiling on a cylinder, *Physics of Fluids* 33 (2021) 023307.
- [42] A. Parmigiani, C. Huber, B. Chopard, J. Latt, O. Bachmann, Application of the multi distribution function lattice Boltzmann approach to thermal flows, *European Physical Journal: Special Topics* 171 (2009) 37–43.
- [43] S. A. Nabavizadeh, H. Barua, M. Eshraghi, S. D. Felicelli, A multiple-grid lattice boltzmann method for natural convection under low and high prandtl numbers, *Fluids* 6 (2021).
- [44] S. Suga, Numerical Schemes Obtained From Lattice Boltzmann Equations for Advection Diffusion Equations,

- International Journal of Modern Physics C 17 (2006) 1563–1577.
- [45] H. Yoshida, M. Nagaoka, Multiple-relaxation-time lattice Boltzmann model for the convection and anisotropic diffusion equation, *Journal of Computational Physics* 229 (2010) 7774–7795.
- [46] L. Li, C. Chen, R. Mei, J. F. Klausner, Conjugate heat and mass transfer in the lattice Boltzmann equation method, *Physical Review E - Statistical, Nonlinear, and Soft Matter Physics* 89 (2014).
- [47] H. Yoshida, T. Kobayashi, H. Hayashi, T. Kinjo, H. Washizu, K. Fukuzawa, Boundary condition at a two-phase interface in the lattice Boltzmann method for the convection-diffusion equation, *Physical Review E - Statistical, Nonlinear, and Soft Matter Physics* 90 (2014) 13303.
- [48] H. Karani, C. Huber, Lattice Boltzmann formulation for conjugate heat transfer in heterogeneous media, *Physical Review E - Statistical, Nonlinear, and Soft Matter Physics* 91 (2015) 906–919.
- [49] S. Chen, B. Yang, C. Zheng, A lattice Boltzmann model for heat transfer in heterogeneous media, *International Journal of Heat and Mass Transfer* 102 (2016) 637–644.
- [50] S. Chen, Y. Yan, W. Gong, A simple lattice Boltzmann model for conjugate heat transfer research, *International Journal of Heat and Mass Transfer* 107 (2017) 862–870.
- [51] H. B. Huang, X. Y. Lu, M. C. Sukop, Numerical study of lattice Boltzmann methods for a convection-diffusion equation coupled with Navier-Stokes equations, *Journal of Physics A: Mathematical and Theoretical* 44 (2011).
- [52] P. Asinari, Generalized local equilibrium in the cascaded lattice Boltzmann method, *Physical Review E - Statistical, Nonlinear, and Soft Matter Physics* 78 (2008) 1–5.
- [53] E. Yahia, W. Schupbach, K. N. Premnath, Three-dimensional central moment lattice boltzmann method on a cuboid lattice for anisotropic and inhomogeneous flows, *Fluids* 6 (2021) 326.
- [54] F. Hajabdollahi, K. N. Premnath, S. W. Welch, Cascaded lattice Boltzmann method based on central moments for axisymmetric thermal flows including swirling effects, *International Journal of Heat and Mass Transfer* 128 (2019) 999–1016.
- [55] M. Matyka, M. Dzikowski, Memory-efficient Lattice Boltzmann Method for low Reynolds number flows, *Computer Physics Communications* 267 (2021) 108044.
- [56] M. Bouzidi, M. Firdaouss, P. Lallemand, Momentum transfer of a Boltzmann-lattice fluid with boundaries, *Physics of Fluids* 13 (2001) 3452–3459.
- [57] F. Dubois, P. Lallemand, Towards higher order lattice boltzmann schemes, *Journal of Statistical Mechanics: Theory and Experiment* 2009 (2009).
- [58] D. d’Humières, I. Ginzburg, Viscosity independent numerical errors for lattice boltzmann models: from recurrence equations to “magic” collision numbers, *Computers & Mathematics with Applications* 58 (2009) 823–840.
- [59] L. Li, R. Mei, J. F. Klausner, Boundary conditions for thermal lattice Boltzmann equation method, *Journal of Computational Physics* 237 (2013) 366–395.
- [60] F. Dubois, P. Lallemand, M. M. Tekitek, On anti bounce back boundary condition for lattice Boltzmann schemes, *Computers and Mathematics with Applications* (2019).
- [61] F. M. Elseid, S. W. Welch, K. N. Premnath, A cascaded lattice boltzmann model for thermal convective flows with local heat sources, *International Journal of Heat and Fluid Flow* 70 (2018) 279–298.
- [62] F. Hajabdollahi, K. N. Premnath, Central moments-based cascaded lattice Boltzmann method for thermal convective flows in three-dimensions, *International Journal of Heat and Mass Transfer* 120 (2018) 838–850.
- [63] Q. Li, K. H. Luo, Y. L. He, Y. J. Gao, W. Q. Tao, Coupling lattice Boltzmann model for simulation of thermal flows on standard lattices, *Physical Review E - Statistical, Nonlinear, and Soft Matter Physics* 85 (2012) 1–16.
- [64] R. Huang, H. Wu, P. Cheng, A new lattice Boltzmann model for solid-liquid phase change, *International Journal of Heat and Mass Transfer* 59 (2013) 295–301.
- [65] A. Grucelski, J. Pozorski, Lattice Boltzmann simulations of heat transfer in flow past a cylinder and in simple porous media, *International Journal of Heat and Mass Transfer* 86 (2015) 139–148.
- [66] J. McCullough, S. Aminossadati, B. Jones, C. Leonardi, J. Williams, Lattice Boltzmann methods for the simulation of heat transfer in particle suspensions, *International Journal of Heat and Fluid Flow* 62 (2016) 150–165.
- [67] J. H. Lu, H. Y. Lei, C. S. Dai, A lattice Boltzmann algorithm for simulating conjugate heat transfer through virtual heat capacity correction, *International Journal of Thermal Sciences* 116 (2017) 22–31.
- [68] J. McCullough, C. Leonardi, B. Jones, S. Aminossadati, J. Williams, Investigation of local and non-local lattice Boltzmann models for transient heat transfer between non-stationary, disparate media, *Computers and Mathematics with Applications* (2018) 1–21.
- [69] J. Wang, D. Wang, P. Lallemand, L. S. Luo, Lattice Boltzmann simulations of thermal convective flows in two dimensions, *Computers and Mathematics with Applications* 65 (2013) 262–286.
- [70] Z. Chai, B. Shi, Z. Guo, A Multiple-Relaxation-Time Lattice Boltzmann Model for General Nonlinear Anisotropic Convection–Diffusion Equations, *Journal of Scientific Computing* 69 (2016) 355–390.
- [71] S. Cui, N. Hong, B. Shi, Z. Chai, Discrete effect on the halfway bounce-back boundary condition of multiple-relaxation-time lattice Boltzmann model for convection-diffusion equations, *Physical Review E* 93 (2016) 43311.
- [72] L. Fei, K. H. Luo, C. Lin, Q. Li, Modeling incompressible thermal flows using a central-moments-based lattice

- Boltzmann method, *International Journal of Heat and Mass Transfer* 120 (2018) 624–634.
- [73] L. Fei, K. H. Luo, Q. Li, Three-dimensional cascaded lattice Boltzmann method: Improved implementation and consistent forcing scheme, *Physical Review E* 97 (2018) 053309.
- [74] A. De Rosis, K. H. Luo, Role of higher-order Hermite polynomials in the central-moments-based lattice Boltzmann framework, *Physical Review E* 99 (2019).
- [75] G. Gruszczyński, T. Mitchell, C. Leonardi, L.-W. Ł., T. Barber, A cascaded phase-field lattice Boltzmann model for the simulation of incompressible, immiscible fluids with high density contrast, *Computers & Mathematics with Applications* (2019).
- [76] B. Chopard, J. L. Falcone, J. Latt, The lattice Boltzmann advection-diffusion model revisited, *The European Physical Journal Special Topics* 171 (2009) 245–249.
- [77] Q. Liu, Y. L. He, D. Li, Q. Li, Non-orthogonal multiple-relaxation-time lattice Boltzmann method for incompressible thermal flows, *International Journal of Heat and Mass Transfer* 102 (2016) 1334–1344.
- [78] I. V. Karlin, D. Sichau, S. S. Chikatamarla, Consistent two-population lattice Boltzmann model for thermal flows, *Physical Review E - Statistical, Nonlinear, and Soft Matter Physics* 88 (2013) 1–13.
- [79] A. Xu, L. Shi, T. S. Zhao, Accelerated lattice Boltzmann simulation using GPU and OpenACC with data management, *International Journal of Heat and Mass Transfer* 109 (2017) 577–588.
- [80] J. H. Lu, H. Y. Lei, C. S. Dai, An optimal two-relaxation-time lattice Boltzmann equation for solid-liquid phase change: The elimination of unphysical numerical diffusion, *International Journal of Thermal Sciences* 135 (2019) 17–29.
- [81] Y. Shi, T. S. Zhao, Z. L. Guo, Thermal lattice Bhatnagar-Gross-Krook model for flows with viscous heat dissipation in the incompressible limit, *Physical Review E - Statistical Physics, Plasmas, Fluids, and Related Interdisciplinary Topics* 70 (2004) 10.
- [82] O. Zikanov, *Essential computational fluid dynamics*, John Wiley & Sons, 2019.
- [83] L. Fei, K. H. Luo, Consistent forcing scheme in the cascaded lattice Boltzmann method, *Physical Review E* 96 (2017).
- [84] L. Fei, K. H. Luo, Q. Li, Three-dimensional cascaded lattice Boltzmann method: Improved implementation and consistent forcing scheme, *Physical Review E* 97 (2018) 1–12.
- [85] I. Ginzburg, Generic boundary conditions for lattice Boltzmann models and their application to advection and anisotropic dispersion equations, *Advances in Water Resources* 28 (2005) 1196–1216.
- [86] I. Ginzburg, F. Verhaeghe, D. D’Humières, Two-relaxation-time Lattice Boltzmann scheme: About parametrization, velocity, pressure and mixed boundary conditions, *Communications in Computational Physics* 3 (2008) 427–478.
- [87] B. Servan-Camas, F. T. Tsai, Lattice Boltzmann method with two relaxation times for advection-diffusion equation: Third order analysis and stability analysis, *Advances in Water Resources* 31 (2008) 1113–1126.
- [88] I. Ginzburg, D. D’Humières, A. Kuzmin, Optimal stability of advection-diffusion lattice Boltzmann models with two relaxation times for positive/negative equilibrium, *Journal of Statistical Physics* 139 (2010) 1090–1143.
- [89] A. Kuzmin, I. Ginzburg, A. A. Mohamad, The role of the kinetic parameter in the stability of two-relaxation-time advection-diffusion lattice Boltzmann schemes, *Computers and Mathematics with Applications* 61 (2011) 3417–3442.
- [90] C. Pan, L. S. Luo, C. T. Miller, An evaluation of lattice Boltzmann schemes for porous medium flow simulation, *Computers and Fluids* 35 (2006) 898–909.
- [91] S. Khirevich, I. Ginzburg, U. Tallarek, Coarse-and fine-grid numerical behavior of MRT/TRT lattice-Boltzmann schemes in regular and random sphere packings, *Journal of Computational Physics* 281 (2015) 708–742.
- [92] D. D’Humières, I. Ginzburg, Viscosity independent numerical errors for Lattice Boltzmann models: From recurrence equations to "magic" collision numbers, *Computers and Mathematics with Applications* 58 (2009) 823–840.
- [93] I. Ginzburg, F. Verhaeghe, D. d’Humières, Study of simple hydrodynamic solutions with the two-relaxation-times lattice Boltzmann scheme, *Communications in computational physics* 3 (2008) 519–581.
- [94] S. Izquierdo, N. Fueyo, Characteristic nonreflecting boundary conditions for open boundaries in lattice Boltzmann methods, *Physical Review E - Statistical, Nonlinear, and Soft Matter Physics* 78 (2008).
- [95] X. He, Q. Zou, L. S. Luo, M. Dembo, Analytic solutions of simple flows and analysis of nonslip boundary conditions for the lattice Boltzmann BGK model, *Journal of Statistical Physics* 87 (1997) 115–136.
- [96] J. Latt, B. Chopard, O. Malaspina, M. Deville, A. Michler, Straight velocity boundaries in the lattice Boltzmann method, *Physical Review E - Statistical, Nonlinear, and Soft Matter Physics* 77 (2008).
- [97] A. A. Mohamad, S. Succi, A note on equilibrium boundary conditions in lattice Boltzmann fluid dynamic simulations, in: *European Physical Journal: Special Topics*, volume 171, Springer-Verlag, 2009, pp. 213–221.
- [98] Ł. Łaniewski-Wołk, J. Rokicki, Adjoint Lattice Boltzmann for topology optimization on multi-GPU architecture, *Computers and Mathematics with Applications* 71 (2016) 833–848.
- [99] Ł. Łaniewski-Wołk, M. Dzikowski, D. Sashko, T. Mitchell, G. Gruszczyński, PabloOb, R. M., R. W., G. T., bhil23, M. J., de Waard C., franjesus, *CFD-GO/TCLB: Version 6.5*, 2020.

- [100] I. Ginzburg, Equilibrium-type and link-type lattice boltzmann models for generic advection and anisotropic-dispersion equation, *Advances in Water resources* 28 (2005) 1171–1195.
- [101] Q. Zou, X. He, On pressure and velocity boundary conditions for the lattice boltzmann bgk model, *Physics of Fluids* 9 (1997) 1591–1598.
- [102] Q. Lou, Z. Guo, B. Shi, Evaluation of outflow boundary conditions for two-phase lattice Boltzmann equation, *Physical Review E - Statistical, Nonlinear, and Soft Matter Physics* 87 (2013) 1–16.
- [103] Z. Guo, C. Zheng, B. Shi, Discrete lattice effects on the forcing term in the lattice Boltzmann method, *Physical Review E - Statistical Physics, Plasmas, Fluids, and Related Interdisciplinary Topics* 65 (2002) 6.
- [104] L. Fei, K. H. Luo, Consistent forcing scheme in the cascaded lattice Boltzmann method, *Physical Review E* 96 (2017) 053307. Publisher: American Physical Society.
- [105] L. Fei, K. H. Luo, Q. Li, Three-dimensional cascaded lattice Boltzmann method: Improved implementation and consistent forcing scheme, *Physical Review E* 97 (2018) 053309. Publisher: American Physical Society.
- [106] R. Huang, H. Wu, N. A. Adams, Eliminating cubic terms in the pseudopotential lattice Boltzmann model for multiphase flow, *Physical Review E* 97 (2018) 53308.
- [107] A. De Rosi, R. Huang, C. Coreixas, Universal formulation of central-moments-based lattice Boltzmann method with external forcing for the simulation of multiphysics phenomena, *Physics of Fluids* 31 (2019) 117102.
- [108] G. Gruszczyński, T. Mitchell, C. Leonardi, T. Barber, et al., A cascaded phase-field lattice boltzmann model for the simulation of incompressible, immiscible fluids with high density contrast, *Computers & Mathematics with Applications* 79 (2020) 1049–1071.
- [109] R. Fučík, R. Straka, Equivalent finite difference and partial differential equations for the lattice Boltzmann method, *Computers and Mathematics with Applications* 90 (2021) 96–103.
- [110] G. Gruszczyński, M. Dzikowski, L. Łaniewski-Woźń, On recovering the second-order convergence of the lattice boltzmann method with reaction-type source terms, *arXiv* (2021).